Petersburg Nuclear Physics Institute of NRC «Kurchatov Institute»

Flat bands, baryon asymmetry of Universe, and the violation of time-reversal symmetry

V. R. Shaginyan

Structure of Presentation

- Particle-Hole (P-H) symmetry in Universe and Landau Fermi Liquid
- Fundamental Properties of Strongly Correlated Fermi Systems
- and flat bands
- Asymmetrical Conductivity and the P-H violation in Strongly Correlated Fermi Systems
- Matter-Antimatter asymmetry in Universe

The asymmetry between matter and antimatter is one of the fundamental puzzles in modern physics. In the Big Bang, equal amounts of matter and antimatter should have been created, and would have annihilated each other except that some kind of symmetry breaking between particles and antiparticles seems have led to the disappearance of antiparticles at an early stage in the history of the Universe.

The Universe seems to be made of matter rather than antimatter. But some theories of cosmology does not exclude the possibility of there being small regions of antimatter out there. However, recent observations show no sign of antihelium in cosmic rays, setting an even lower limit on the possible abundance of antimatter (K. Abe et al. Phys. Rev. Lett. 108, 131301; 2012).

The obtained result has revealed no antihelium in the cosmic rays, implying that antihelium is at least ten million (10^{-7}) times less abundant than its normal matter twin.

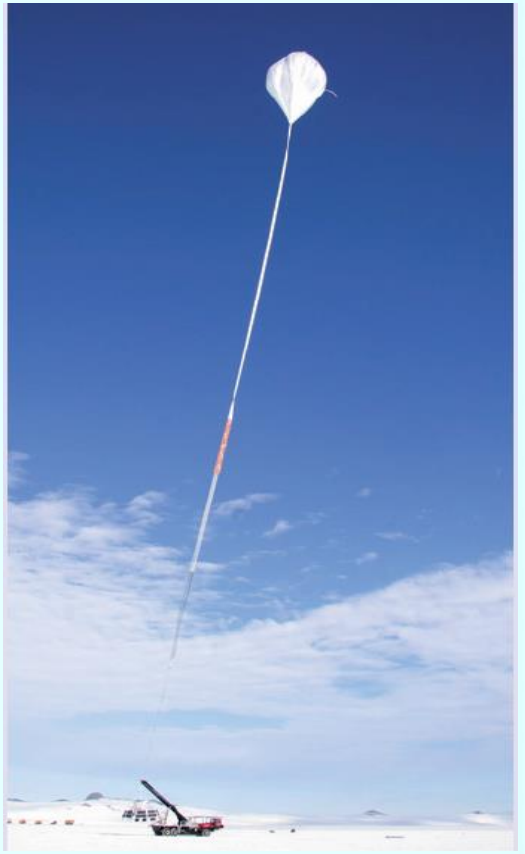

Since 1993, Balloon-borne Experiment with a Superconducting Spectrometer (pictured) has been hunting for signs of antihelium in cosmic rays.

I. Georgescu, Nature Physics, 8**, 362** (2012).

Specific heat (C) is the measurable physical quantity that characterizes the amount of heat required to change a substance's temperature by a given amount.

For gases, heat capacity never falls below the minimum of 3⁄2 R per mole (R is the ideal gas constant), since the kinetic energy of gas molecules is always available to store this much heat energy. For room temperatures in solids, heat capacity does not depend on temperature.

It is quantum mechanics, also known as **quantum physics** or **quantum theory that gives explanations of the heat capacity C at room and cryogenic temperatures .**

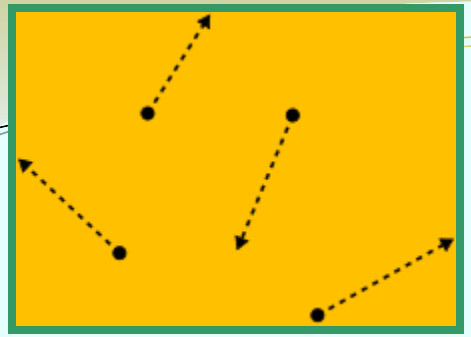

Gas phase particles (atoms, molecules, or ions) move around freely, therefore the kinetic energy of gas molecules is always available to store the energy.

Eruption of Mount Redoubt, Alaska, illustrates real gases in Nature.

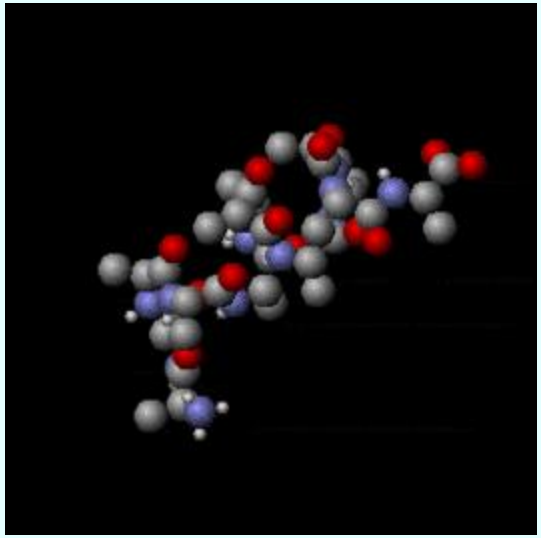

$$C = const$$

The phonon contribution to the specific heat in a solid.

Ludwig Boltzmann

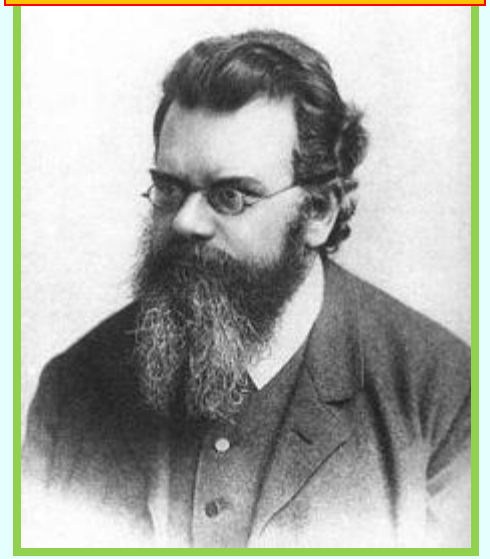

Almost two hundred years ago, Pierre Dulong and Alexis Petit discovered experimentally that the specific heat C of a crystal is close to constant independent of the temperature T. Later, Ludwig Boltzmann reproduced the results of Dulong and Petit quantitatively. However, subsequent measurements at low temperatures demonstrated that C drops rapidly as T is lowered toward zero, in sharp contrast to Boltzmann's theory.

$$C_{electron} = \gamma T$$

$$C_{phonon} = \gamma_1 T^3$$

It was a real crisis.

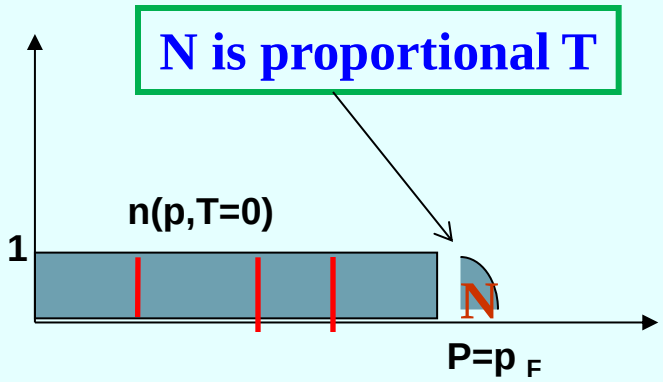

Quantum mechanics says electrons of a metal are responsible for the specific heat. At low temperatures these occupy levels P laying below P_F . Only small amount N (proportional to T) of them located above P_F . These N electrons are able to store the heat. As a result, C is *proportional* T.

Refining the model

Fermi Surface

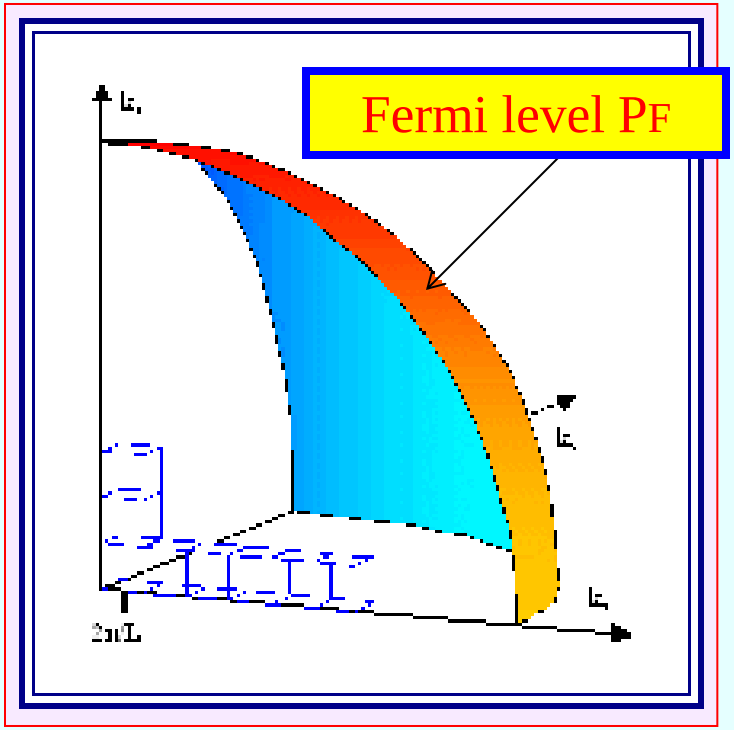

$$C = \gamma T$$

$$\gamma \propto m^*$$

$$\varepsilon(p_F) = \mu.$$

$$\varepsilon(p) - \mu \approx \frac{p_F(p - p_F)}{M^*}.$$

Metal	γ(exp)	γ_0 (free electron)	γ/γ_0
Ag	0.646	0.65	1.00
Cu	0.695	0.50	1.39
Rb	2.41	1.97	1.22
Li	1.63	0.75	2.17

Refining the model

Fermi Liquid

The Landau paradigm

Any weakly excited state of a macroscopic body may be regarded as an Assembly/gas of separate elementary excitations . These behave as quasiparticles with the effective mass M* and define the properties.

The effective mass M* is finite, positive and approximately independent of temperature, magnetic fields etc.

$$C = \gamma T \propto M^* T$$

Metal	γ(exp)	γ_0 (free electron)	γ/γ_0
Ag	0.646	0.65	1.00
Cu	0.695	0.50	1.39
Rb	2.41	1.97	1.22
Li	1.63	0.75	2.17

The calculation of the thermodynamic properties requires a knowledge of the energy spectrum.

The Landau paradigm

Any weakly excited state of a macroscopic body may be regarded as an assembly of separate elementary excitations . These behave as quasiparticles with the effective mass M*.

At the Fermi level the dispersion relation for these is

$$\varepsilon(p,T)-\mu \approx \frac{p_F(p-p_F)}{M^*}.$$

The effective mass M* is finite, positive and approximately independent of temperature, magnetic fields etc.

Landau Fermi liquid support the particle-hole symmetry

The Universe does not

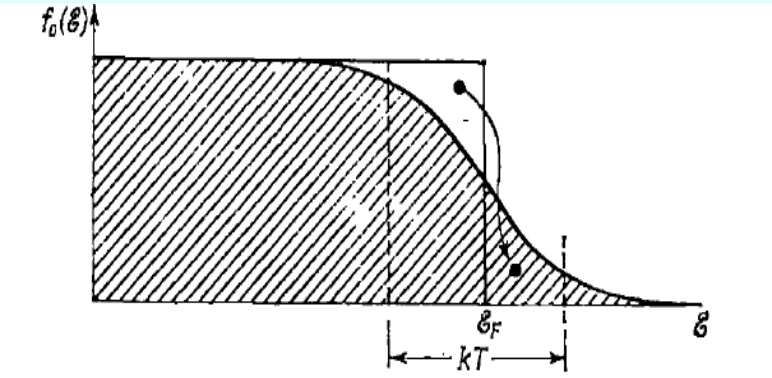

P-H Symmetry

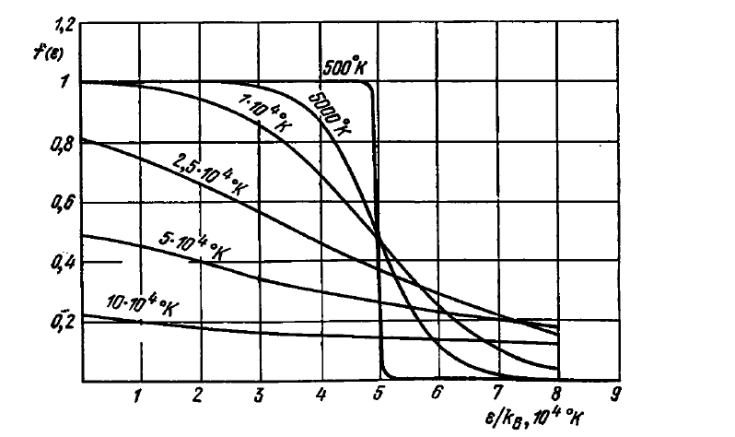

The distribution function at finite temperatures

The weak interaction, violating the P-H symmetry is too weak to support the visible asymmetry

The Landau equation for the effective mass M*

$$\frac{1}{M^*(T,B)} = \frac{1}{M} + \int \frac{\vec{p}_F \vec{p}}{p_F^{\,3}} f(p_F, p) \frac{\partial n(p,T,B)}{\partial p} \frac{d\,\vec{p}}{(2\pi)^3}.$$

$$\frac{1}{M^*(T,B)} = \frac{1}{M^*} + \int \frac{\vec{p}_F \vec{p}}{p_F^{\,3}} f(p_F, p) \frac{\partial\,[n(p,T,B) - n_0(p)]}{\partial p} \frac{d\,\vec{p}}{(2\pi)^3}.$$

The integral I on the r.h.s. is proportional:

$$I \propto \left(\frac{T}{E_F}\right)^2 \propto \left(\frac{\mu_B B}{E_F}\right)^2.$$

At temperatures of a few tens K and fields of a few tens T

$$I \propto \left(\frac{T}{E_F}\right)^2 \propto \left(\frac{\mu_B B}{E_F}\right)^2 \approx 10^{-6}. \longrightarrow M^* = const.$$

Scaling behavior of the Landau Fermi liquid is trivial

$$S(T) \approx \pi^2 \frac{M^* T}{p_F^2}.$$

$$C(T) \approx \pi^2 \frac{M^* T}{p_F^2}$$

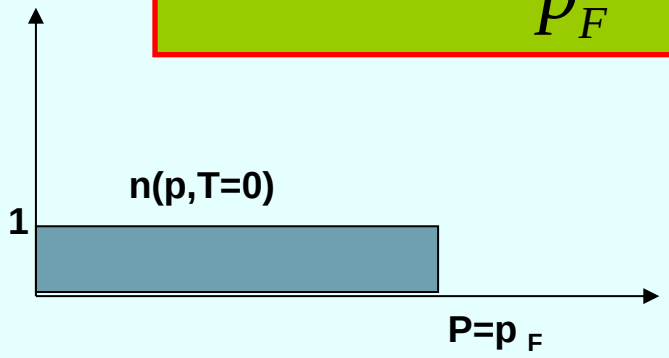

$$M^* = const.$$

$$S(T) = aT, \quad C(T) = \gamma T.$$

Strongly correlated Fermi systems (or heavy-fermion compounds) are fundamental systems in physics that are best studied experimentally, which until very recently have lacked theoretical explanations . We show both analytically and using arguments based entirely on experimental grounds that the data collected on very different strongly correlated Fermi systems have a universal scaling behavior, and materials with strongly correlated fermions can unexpectedly be uniform in their diversity. Our analysis of strongly correlated systems such as HF metals and 2D Fermi systems is in the context of salient experimental results.

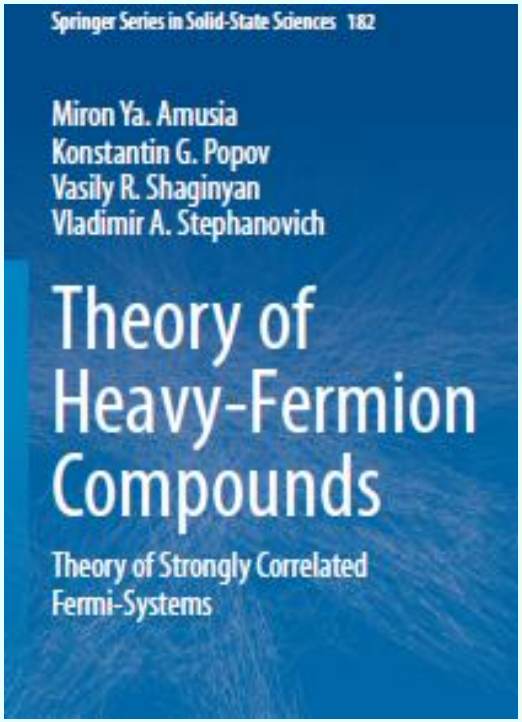

V. R. Shaginyan, M. Ya. Amusia, A. Z. Msezane, and K. G. Popov, Phys. Rep. **492**, 31 (2010).

V.A. Khodel and V.R. Shaginyan, Superfluidity in systems with fermion condensate. JETP Lett. 51, 553 (1990).

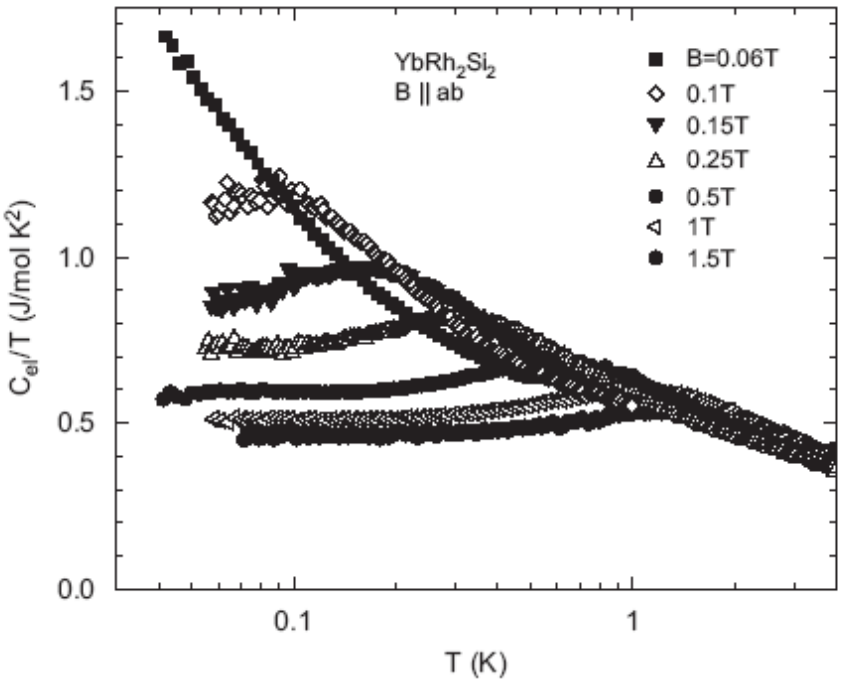

Fig. 2. Electronic specific heat of $YbRh_2Si_2$, C_{el}/T in fields $0.06\,T \leqslant B \leqslant 1.5\,T$.

Quantum phase transitions and the return of crisis

A century later after the first crisis , the very same measurement of the specific heat points to a new crisis with our theories of matter.

$$\alpha \approx -2/3.$$

$$C/T = \gamma \propto M^* \propto T^{\alpha}.$$

N. Oeschler, et. al., Physica B 403 (2008) 1254.

V.R. Shaginyan, M.Ya. Amusia, K.G. Popov,
Phys. Lett. A 373, 2281 (2009).

QUANTUM PHASE TRANSITIONS

Melting argon ice shows the transitions from solid to liquid , and finally to gas.

Phase transitions, such as the solid-liquid transition between ice and water or the liquid-gas transition of boiling water, play a major role in everyday life . All of them take place at finite temperatures, T=Tc.

When T is near T_c, the heat capacity C typically has a power law behavior:

$$C \propto (T - T_c)^{-\alpha}.$$

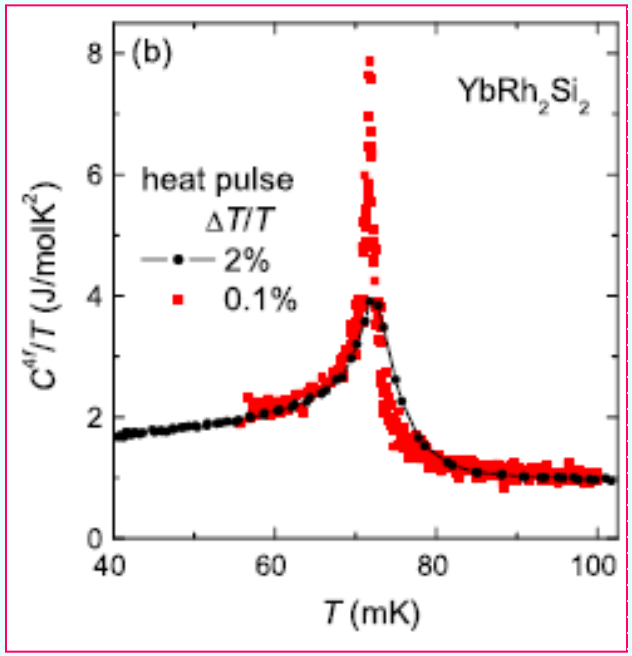

Some phase transition may occur at zero temperature (the critical temperature Tc=0) representing quantum phase transitions.

$$C \propto T^{\beta}.$$

Heavy Fermions

- **Begin by example**:
  - Specific Heat is function of T rather than linear in T
  - ~1000 times larger than expected by Fermi Liquid Theory
  - Implies: m* ~ 1000 times larger or even ***divergent***
- **Interesting Properties**:
  - Heavy Fermion Systems were the first to display NFL behavior.
  - The well-defined quasiparticles determine the thermodynamic and transport properties of strongly correlated Fermi-systems
  - M* becomes a function of temperature, magnetic field, etc
  - They also are an example of "exotic conductivity" and CT violation at macroscopic scale

<u>The studied object</u>: strongly correlated Fermi systems like heavy electron metals.

Blue regions indicate normal metallic behavior. Orange regions indicate anomalous metallic behavior with linear resistivity. The singular quantum critical point at absolute zero produces a wide region of unusual metallic behavior at finite temperatures.

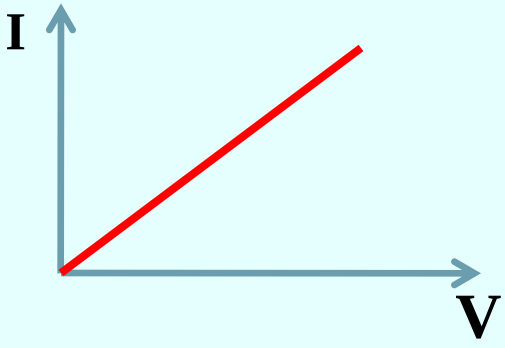

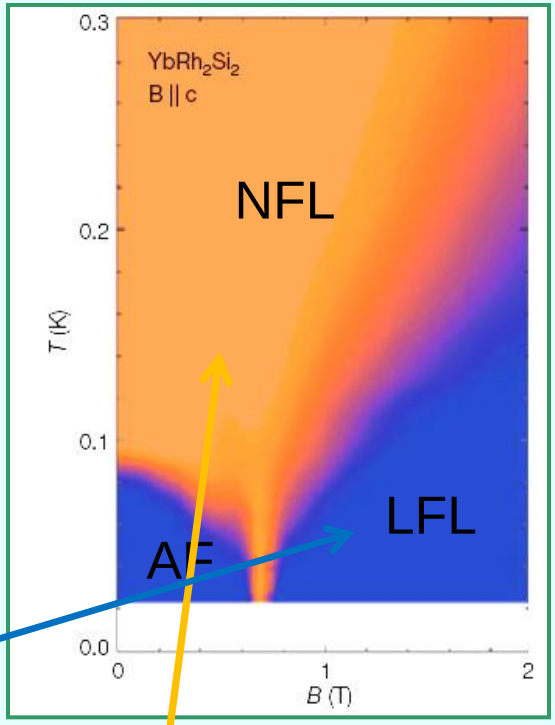

$$\rho = V / I; \quad \rho = \rho_0 + AT^2.$$

$$\rho = \rho_0 + DT.$$

The heat capacity and magnetization of a fluid ^{3}He monolayer adsorbed on graphite plated with a bilayer of HD have been measured in the temperature range 1–60 mK. Approaching the density at which the monolayer solidifies into a $\sqrt{7} \times \sqrt{7}$ commensurate solid, we observe an apparent divergence of the effective mass and magnetization corresponding to a $T = 0$ Mott-Hubbard transition between a 2D Fermi liquid and a magnetically disordered solid. The observations are consistent with the Brinkman-Rice-Anderson-Vollhardt scenario for a metal-insulator transition. We observe a leading order T^2 correction to the linear term in heat capacity.

A.Casey et al., Phys. Rev. Lett. 90, 115301 (2003); M. Neumann, J. Nyeki, J. Saunders, Science 317, 1356 (2007).

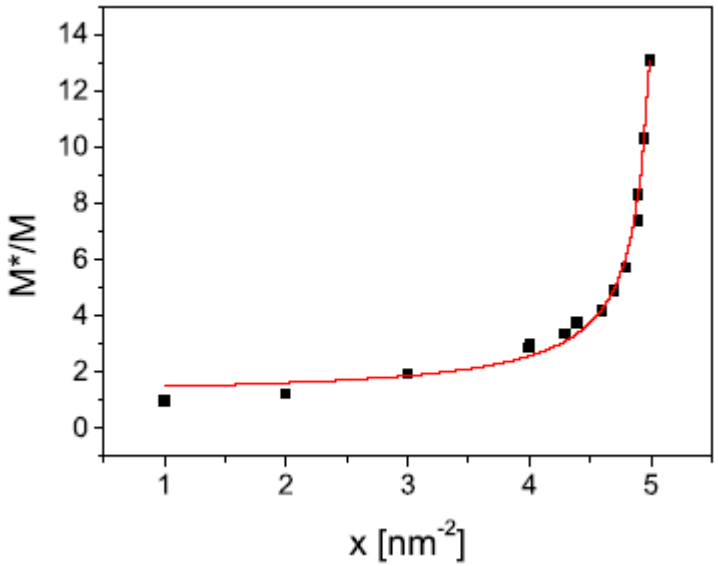

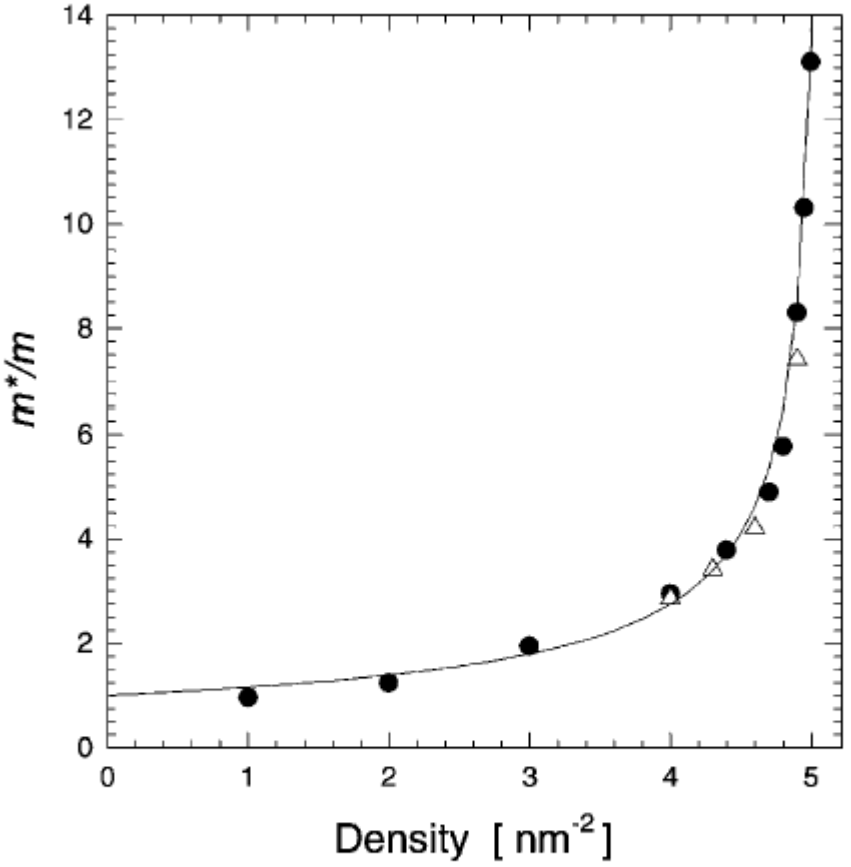

FIG. 2. Effective mass ratio as a function of ^{3}He fluid density inferred from heat capacity (●), magnetization (△), showing apparent divergence. Solid line is fit to data (see text).

$$\chi \propto C/T \propto M^*$$

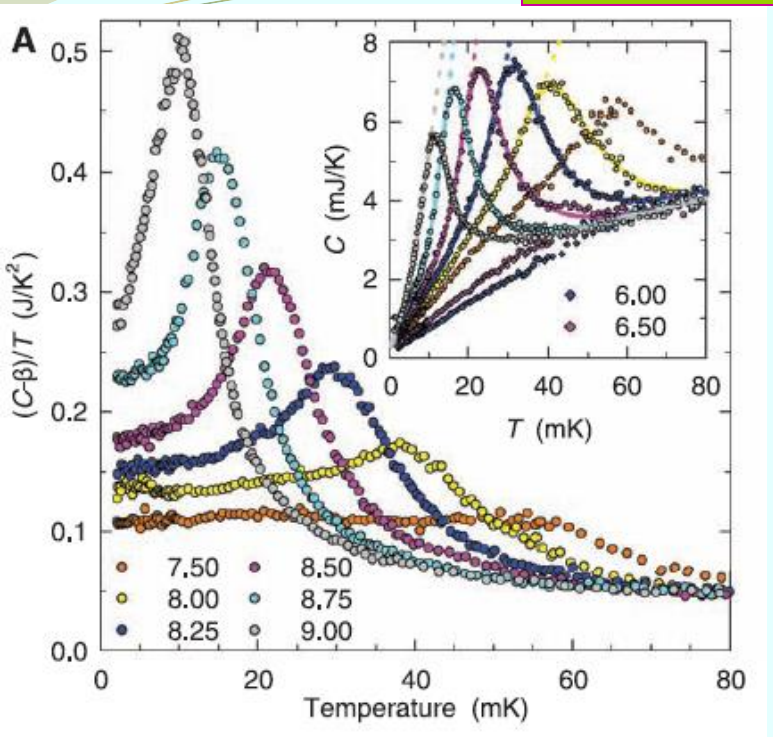

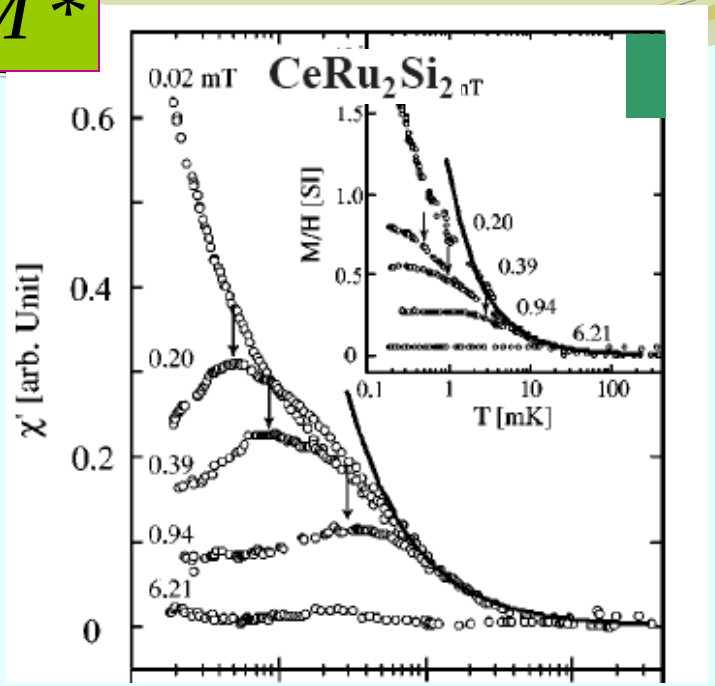

Susceptibility versus T as a function B

The heat capacity C(T)/T versus T as a function of x, 2D 3He

$0.1 \;\; mK \le T_M \le 2 \;\; K.$

$0.02 \;\; mT \le B \le 3 \;\; T.$

$$\frac{M_{^3He}}{M_e} \approx 10^4$$

The heat capacity C(T)/T versus T as a function of B.

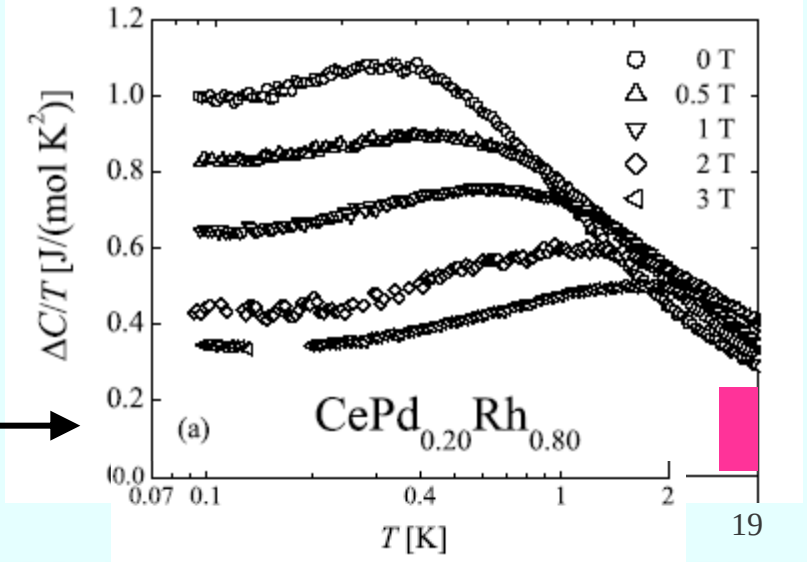

Normal Fermi liquid and FC Fermi liquid are separated by Topological Fermion Condensation Quantum Phase Transition

Normal Fermi liquid

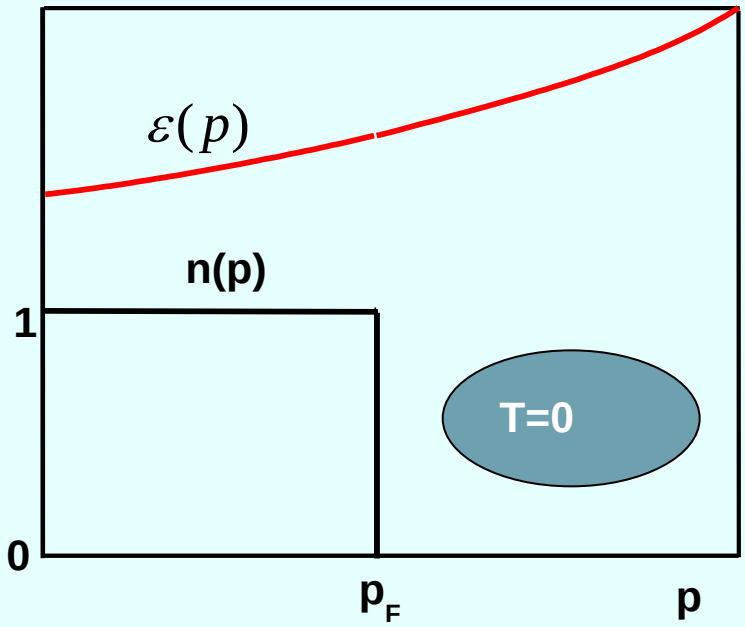

Fermi liquid with FC

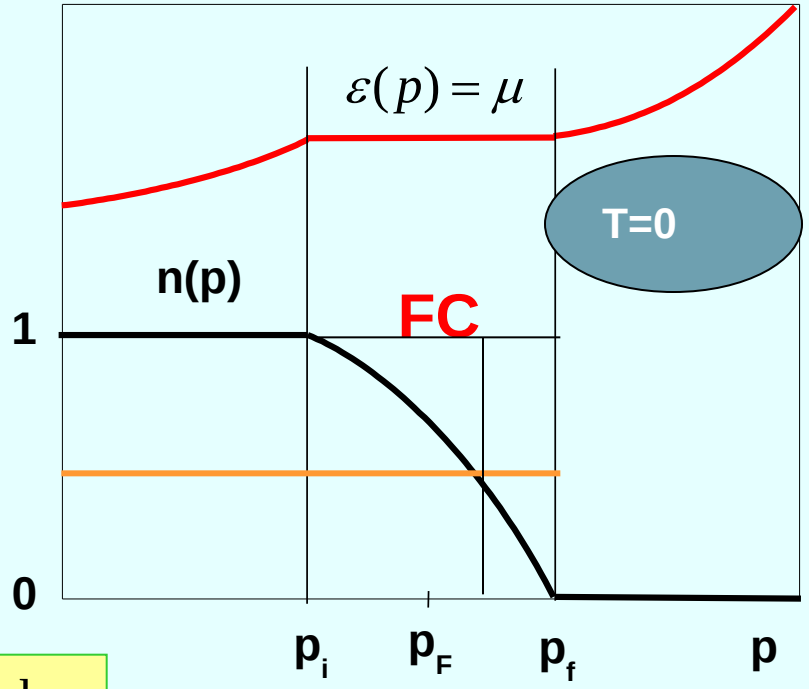

Entropy is given by

$$S[n(\mathbf{p},T)] = -2\int \left[n(\mathbf{p},T)\ln n(\mathbf{p},T) + (1-n(\mathbf{p},T))\ln(1-n(\mathbf{p},T))\right]\frac{d\mathbf{p}}{(2\pi)^3},$$

$$S(T\to 0)\to S_0.$$

$$\frac{1}{M^*(T,B)} = \int \frac{\vec{p}_F \vec{p}}{p_F^{\,3}} f(p_F, p) \frac{\partial\,[n(p,T,B) - n_0(p)]}{\partial p} \frac{d\vec{p}}{(2\pi)^3}.$$

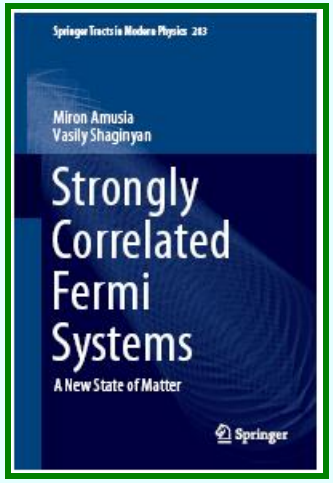

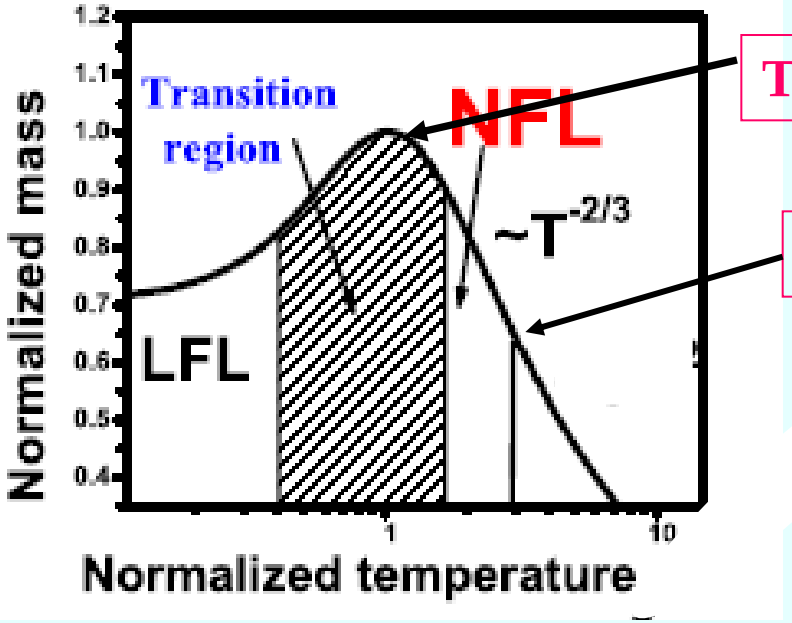

TM

Inflection point T*

An approximate solution of the Landau equation at 1/M*=0.

$$M^*_M(B) \propto (B)^{-2/3}; T_M \propto B.$$

$$M^*(T) \propto T^{-2/3}.$$

$$M^*_N(y) = \frac{M^*(T,B,x)}{M^*_M} \approx \frac{1 + c_1 y^2}{1 + c_2 y^{8/3}}; y = \frac{T}{T_M}.$$

T-dependence of the electronic specific heat C/T of $YbRh_2Si_2$ at different magnetic fields. The values of $(C/T)_{max}$ and T_{max} at B=8 Tesla are shown. The maximum $(C/T)_{max}$ decreases with growing magnetic field B, while T_{max} shifts to higher T reaching 14 K at B=18 Tesla.

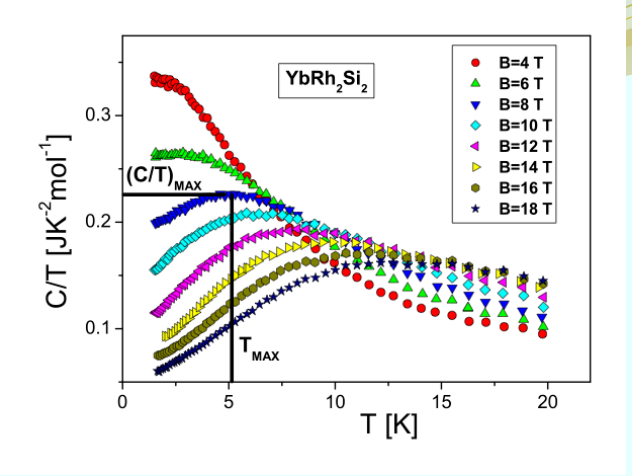

The effective mass M* is finite, positive and independent of temperature, magnetic field, pressure etc.

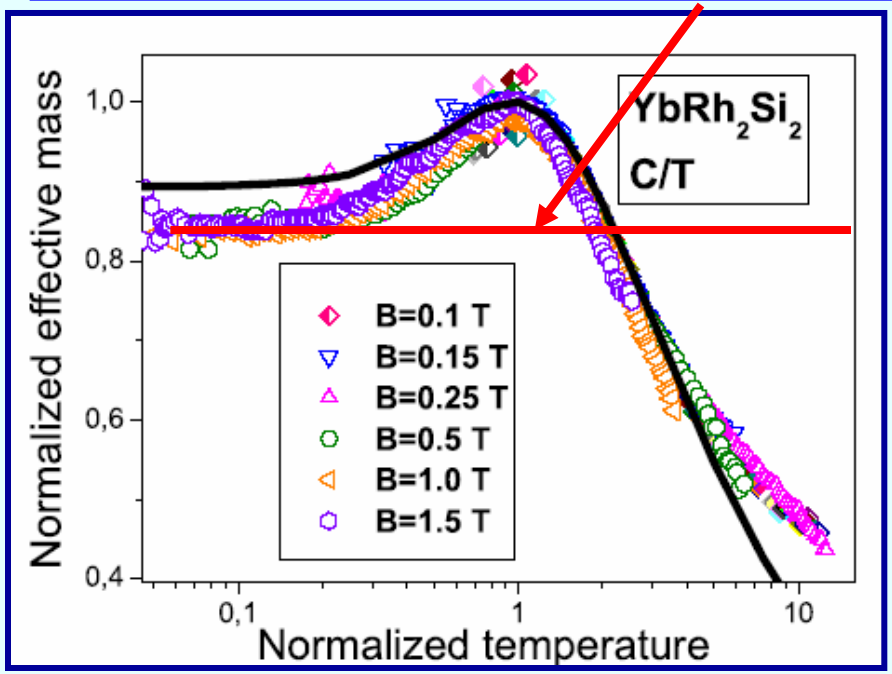

$$C/T = p_F M^*/\pi^2$$

The normalized effective mass extracted from the measurements of the specific heat C/T on YbRh2Si2 in magnetic fields. Our calculations are depicted by the solid curve tracing the scaling behavior.

Entropy versus T as a function of the number density x in 2D 3He

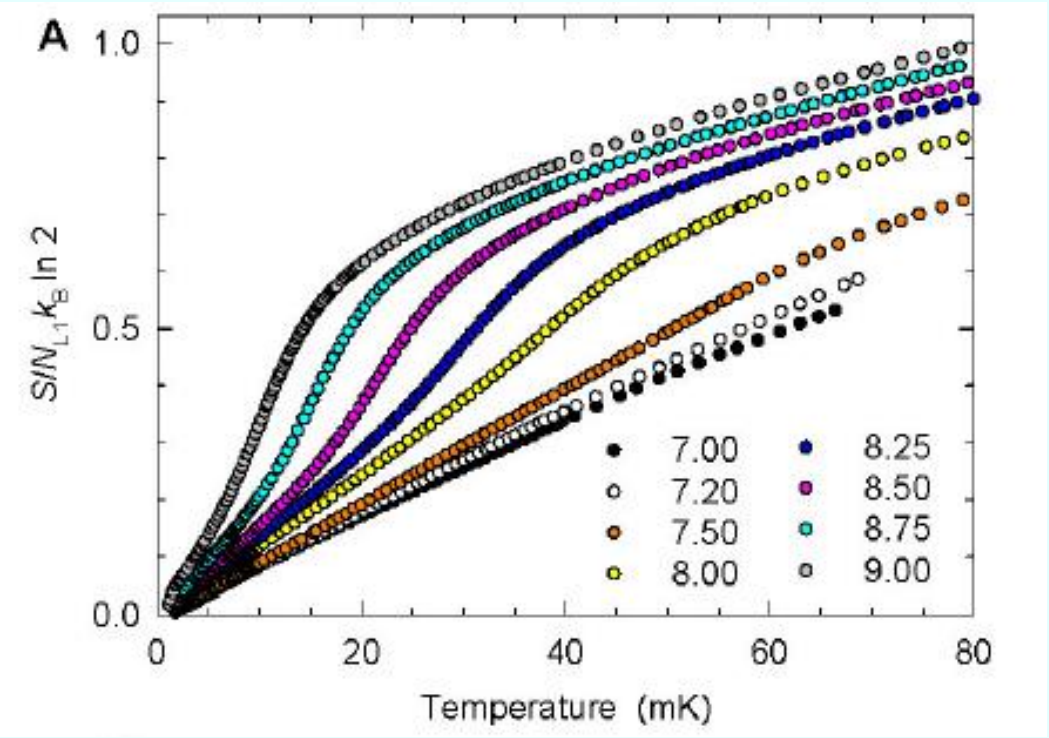

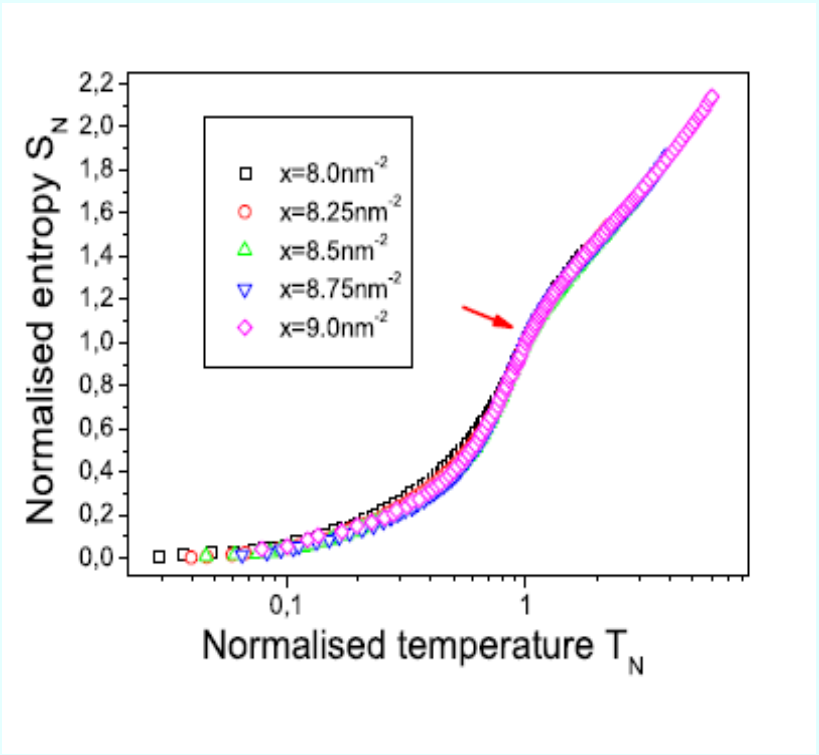

M. Neumann, J. Nyeki, J. Saunders, Science 317, 1356 (2007).

V.R. Shaginyan, et. al., Phys. Rev. Lett. 100 (2008) 096406.

Universal scaling behavior of heavy fermion metals and 2D **3He**

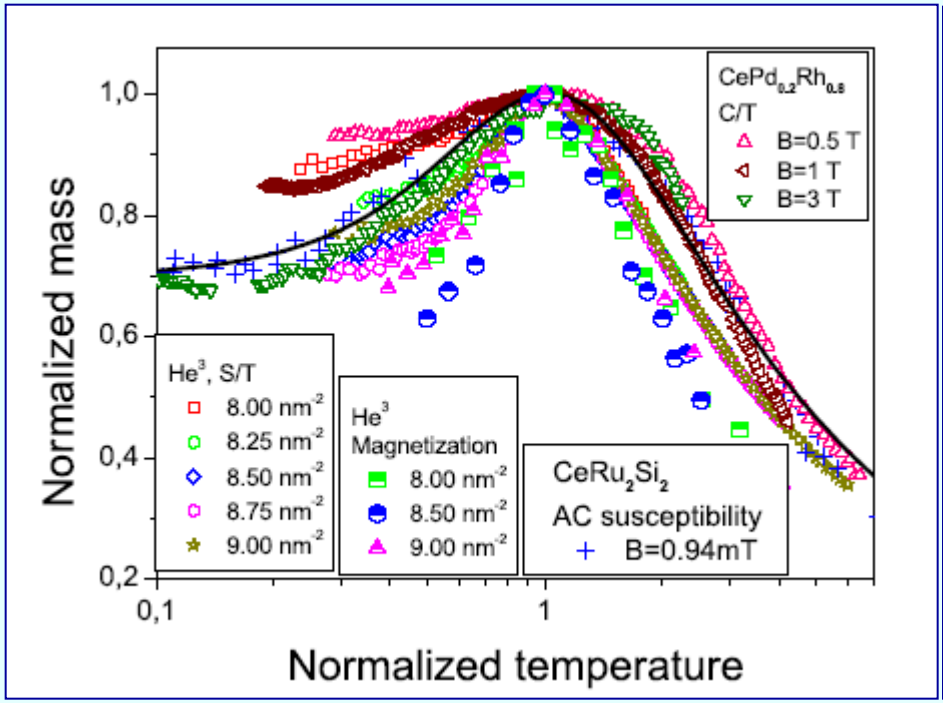

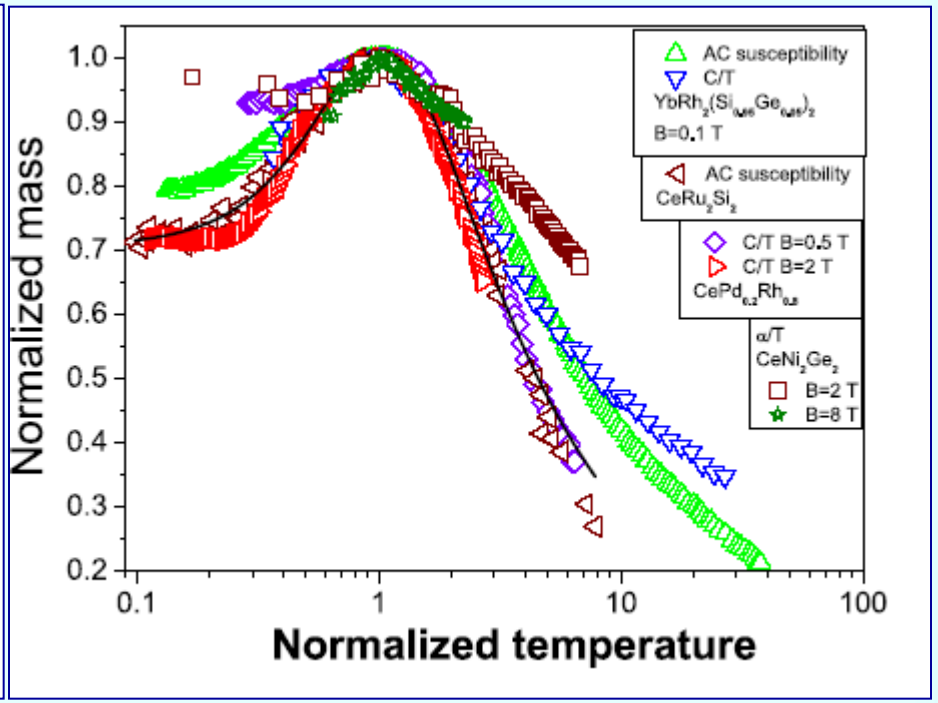

A 4D function describing M* is reduced to a function of a single variable. M* depends on magnetic field, temperature, number density, and the composition. All these parameters can be merged in the single variable.

V.R. Shaginyan, et. al., Phys. Rev. Lett. 100 (2008) 096406.

Exotic quantum spin liquid (QSL) is made with such hypothetic particles as fermionic spinons which carry spin 1/2 and no charge. A great variety of QSL are discovered in theory. The experimental identifying of QSLs heavily depends on theoretical interpretation making the search for the corresponding material to investigate spin liquid a challenge in condensed matter physics.

Mineral Herbertsmithite $ZnCu_3(OH)_6Cl_2$ is an insulator

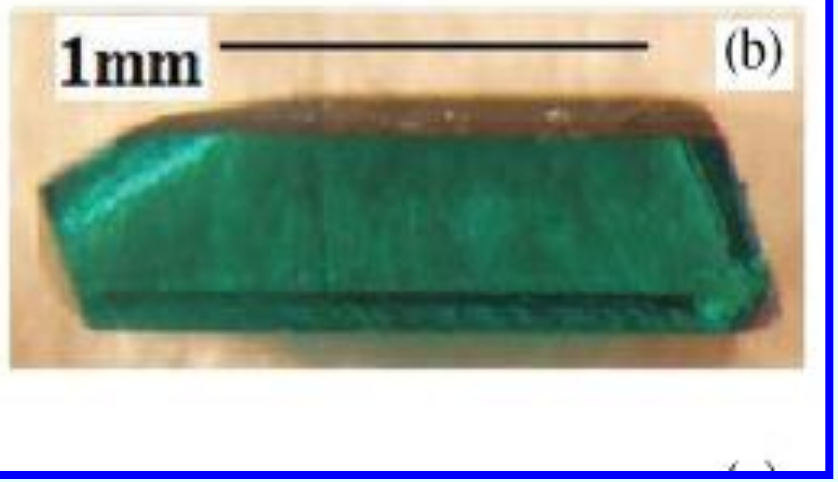

T.T. Han et.al.,
PRB 83, 100402 (2011)

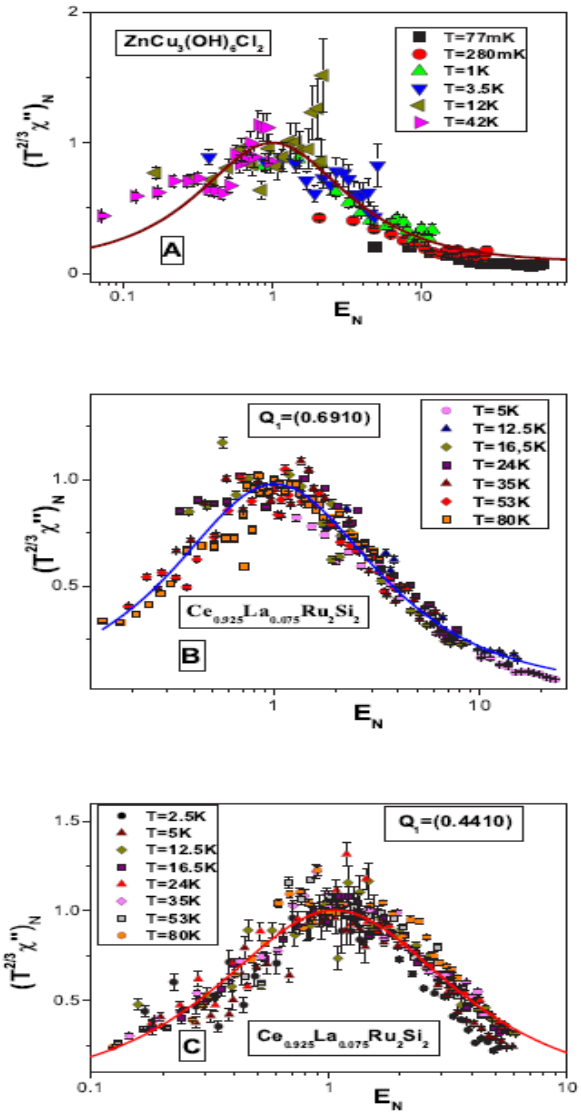

FIG. 2: (color online). The function $(T^{2/3}\chi'')_N$ plotted against the unitless ratio $E_N = \omega/((k_B T)^{2/3} E_{\max})$. The data extracted from measurements on $ZnCu_3(OH)_6Cl_2$ obtained for $0.077 < T < 42$ K [7], Panel A, and on the HF metal $Ce_{0.925}La_{0.075}Ru_2Si_2$ obtained for $2.5 < T < 80$ K at Q_1 [24], Panel B and C, collapse onto a single curve. The solid curves are fits with the function given by Eq. (9).

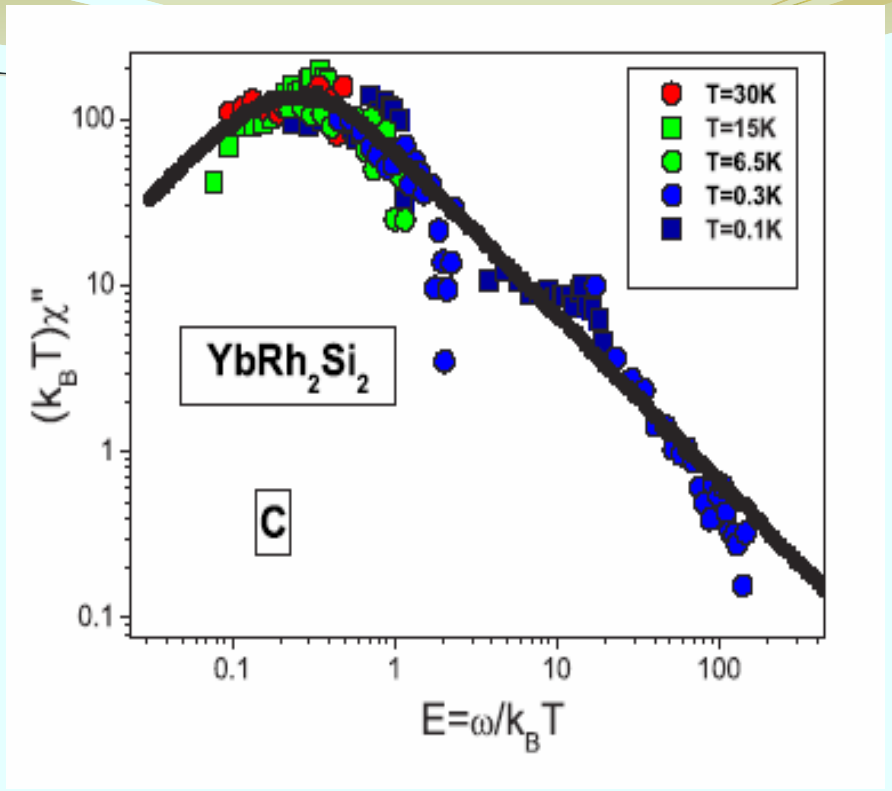

$$T\chi''(T,\omega) \simeq \frac{a_5 E}{1 + a_6 E^2},$$

$$E = \omega/k_B T.$$

$$(T^{2/3}\chi'')_N \simeq \frac{b_1 E_N}{1 + b_2 E_N^2}$$

$$E = \omega/(k_B T)^{2/3}$$

New objects: Quasicrystals

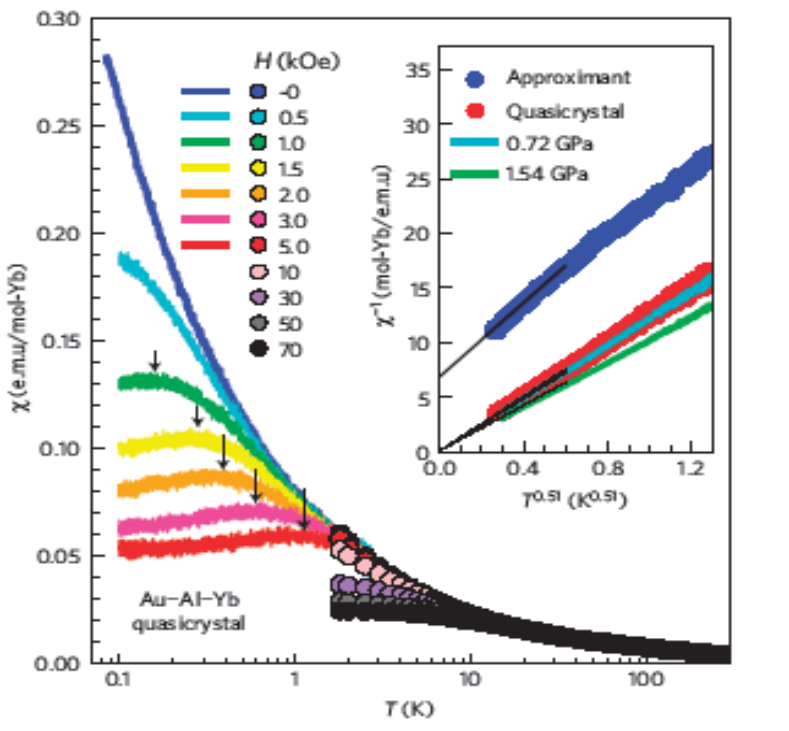

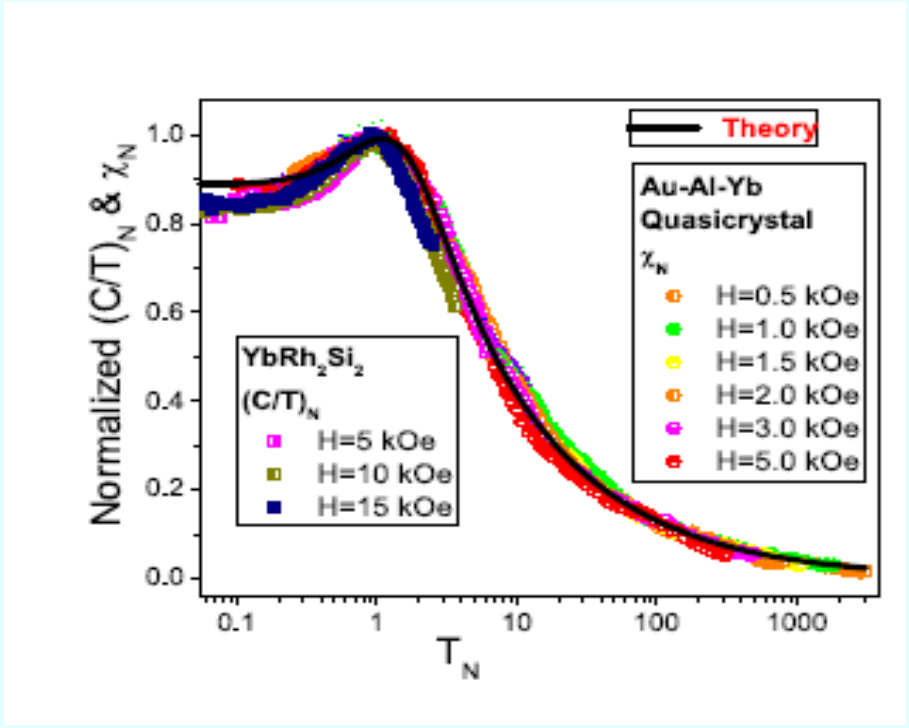

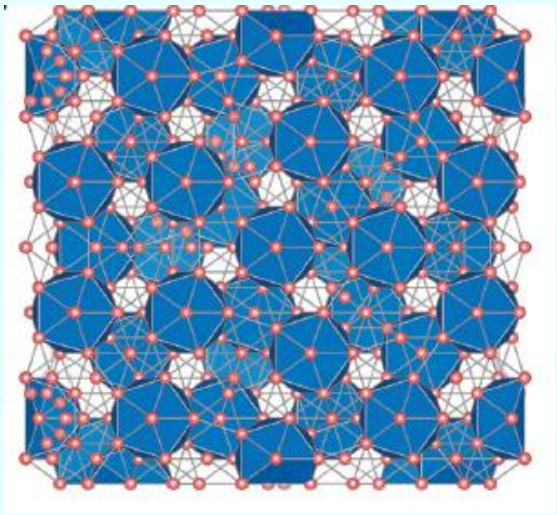

Kazuhiko Deguchi et. al., Natures materials, “Quantum critical state in a magnetic quasicrystal”

$Cd_{5.7}Yb$ quasicrystal

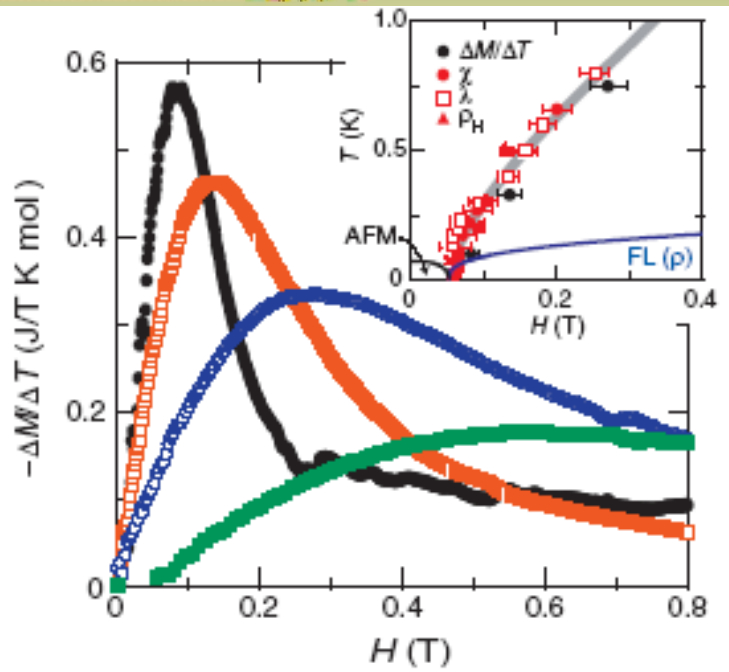

FIG. 3 (color online). Magnetization difference divided by temperature increment $-\Delta M/\Delta T$ (see text) vs magnetic field for $YbRh_2Si_2$ at $T = 0.08$ K (black circles), 0.33 K (red open squares), 0.75 K (blue open circles) and 1.5 K (green squares). Inset: H-T phase diagram of $YbRh_2Si_2$ with the peak positions in $-\Delta M/\Delta T$ (black solid circles) and $T^*(H)$ (gray solid line) as determined from transport and thermodynamic properties (red or gray symbols) [22,23]. The black and blue or dark gray lines represent the phase boundary of the antiferromagnetic (AFM) ground state and crossover to the Fermi-liquid (FL) regime, respectively [22].

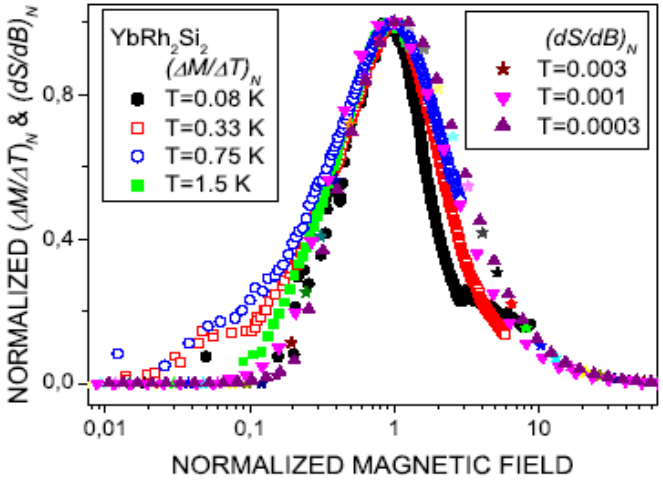

FIG. 5: Normalized magnetization difference divided by temperature increment $(\Delta M/\Delta T)_N$ vs normalized magnetic field at fixed temperatures (listed in the legend in the upper left corner) is extracted from the facts collected on $YbRh_2Si_2$ [20]. Our calculations of the normalized derivative $(dS/dB)_N \simeq (\Delta M/\Delta T)_N$ vs normalized magnetic field are given at fixed dimensionless temperatures T/μ (listed in the legend in the upper right corner). All the data are shown in the geometrical figures depicted in the legends.

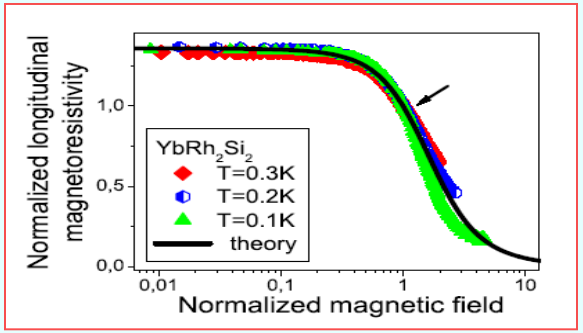

Y. Tokiwa, et. al.,
Phys.Rev.Lett. 102 (2009) 066401.

$$S \propto M^* T$$

$$\frac{\Delta M}{\Delta T} \approx \frac{dM}{dT} = \frac{dS}{dB} \propto \frac{dM^*}{dB}.$$

Landau Fermi liquid support the particle-hole symmetry

The Universe does not

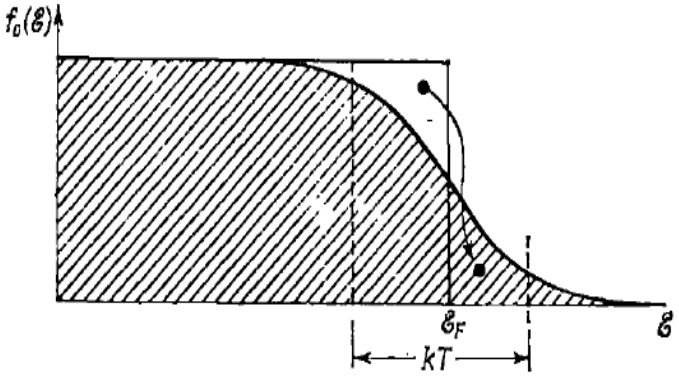

P-H Symmetry

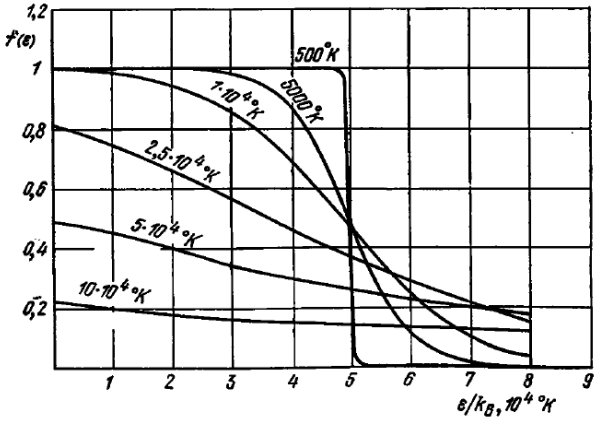

The distribution function at finite temperatures

The weak interaction, violating the P-H symmetry is too weak to support the visible asymmetry

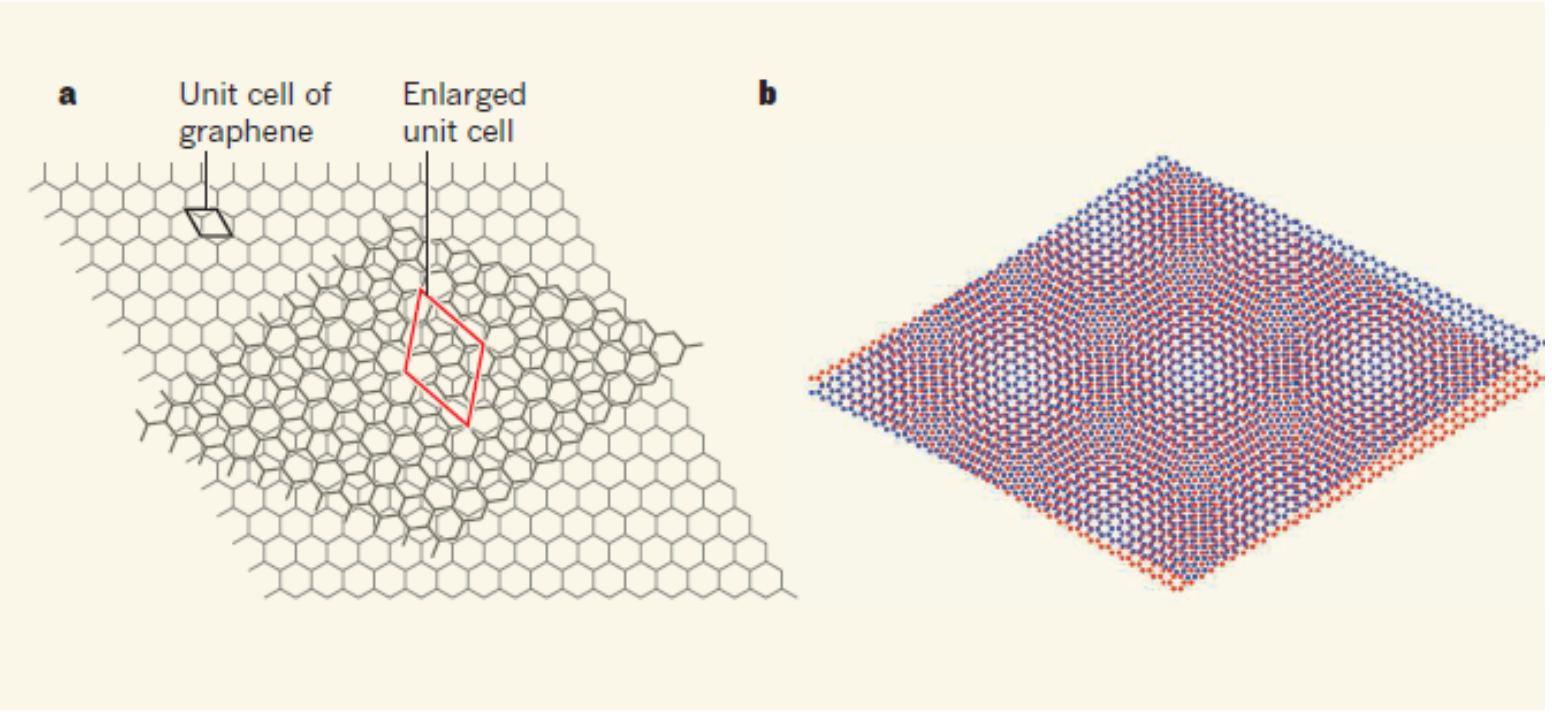

Figure 1 | The effects of rotation in twisted bilayer graphene. **a**, When a graphene bilayer is twisted s
that the top sheet is rotated out of alignment with the lower sheet, the unit cell (the smallest repeating ur
of the material's 2D lattice) becomes enlarged. For large rotations, the electronic band structures of the
two graphene sheets are also rotated out of alignment (not shown). **b**, For small rotation angles, a 'moir
pattern is produced in which the local stacking arrangement varies periodically. Cao *et al.*[1,2] have observ
that, for rotation angles of less than 1.05°, regions in which the atoms are directly above each other (the
lighter regions in the pattern) form narrow electron energy bands, in which electron 'correlation' effects
are enhanced. This results in the generation of a non-conducting state[2] (a Mott insulator), which can be
converted into a superconducting state[1] if charge carriers are added to the graphene system.

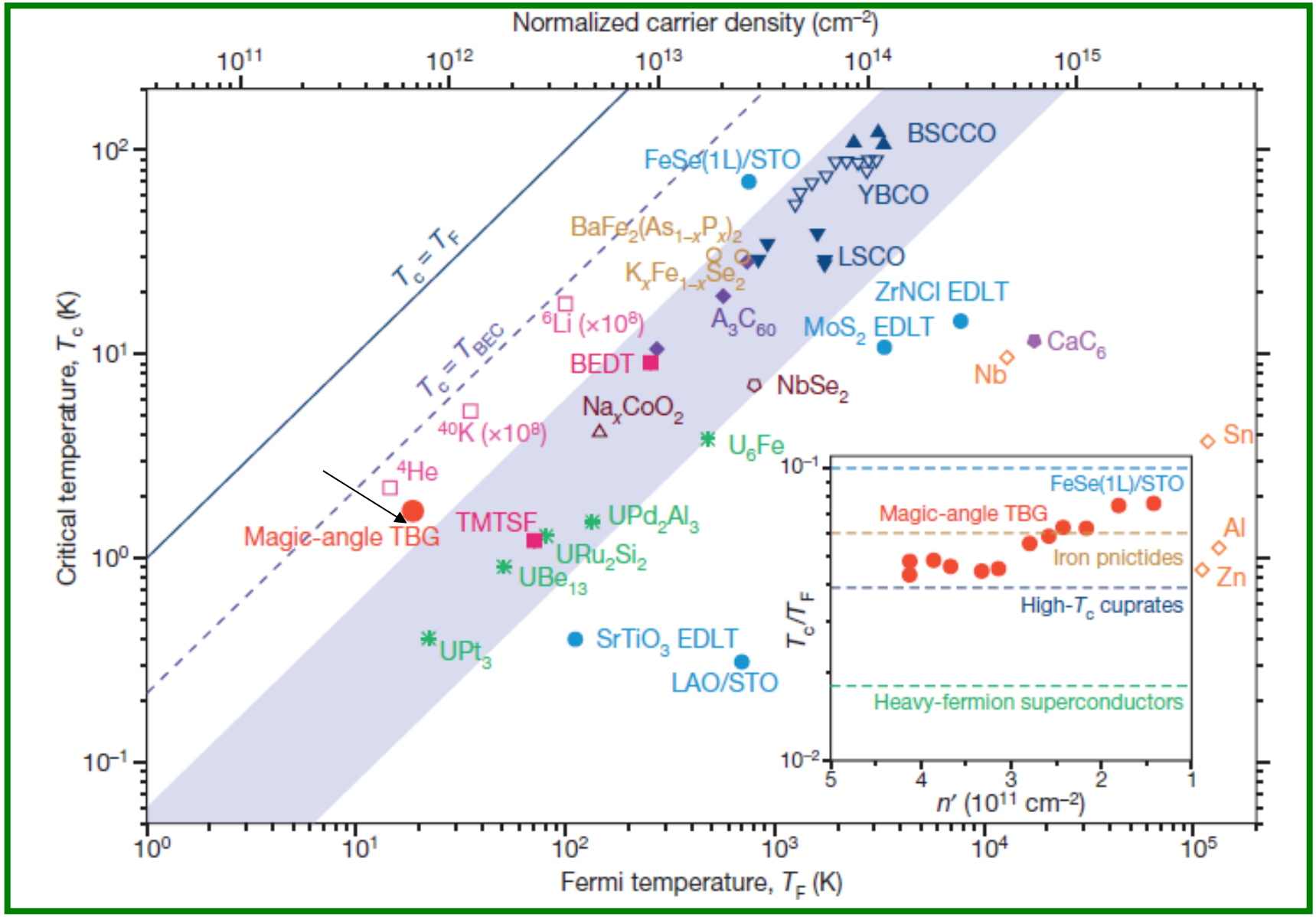
Normalized carrier density (cm^{-2})
10^{11}
10^{12}
10^{13}
10^{14}
10^{15}
Critical temperature, T_c (K)
10^{2}
10^{1}
10^{0}
10^{-1}
$T_c = T_F$
$T_c = T_{BEC}$
BSCCO
FeSe(1L)/STO
YBCO
$BaFe_2(As_{1-x}P_x)_2$
LSCO
$K_xFe_{1-x}Se_2$
ZrNCl EDLT
^{6}Li (×10^8)
A_3C_{60}
MoS_2 EDLT
CaC_6
BEDT
Nb
$NbSe_2$
Na_xCoO_2
^{40}K (×10^8)
U_6Fe
Sn
^{4}He
Magic-angle TBG
TMTSF
UPd_2Al_3
Al
URu_2Si_2
Zn
UBe_{13}
$SrTiO_3$ EDLT
UPt_3
LAO/STO
T_c/T_F
10^{-1}
10^{-2}
FeSe(1L)/STO
Magic-angle TBG
Iron pnictides
High-T_c cuprates
Heavy-fermion superconductors
5
4
3
2
1
n' (10^{11} cm^{-2})
10^{0}
10^{1}
10^{2}
10^{3}
10^{4}
10^{5}
Fermi temperature, T_F (K)

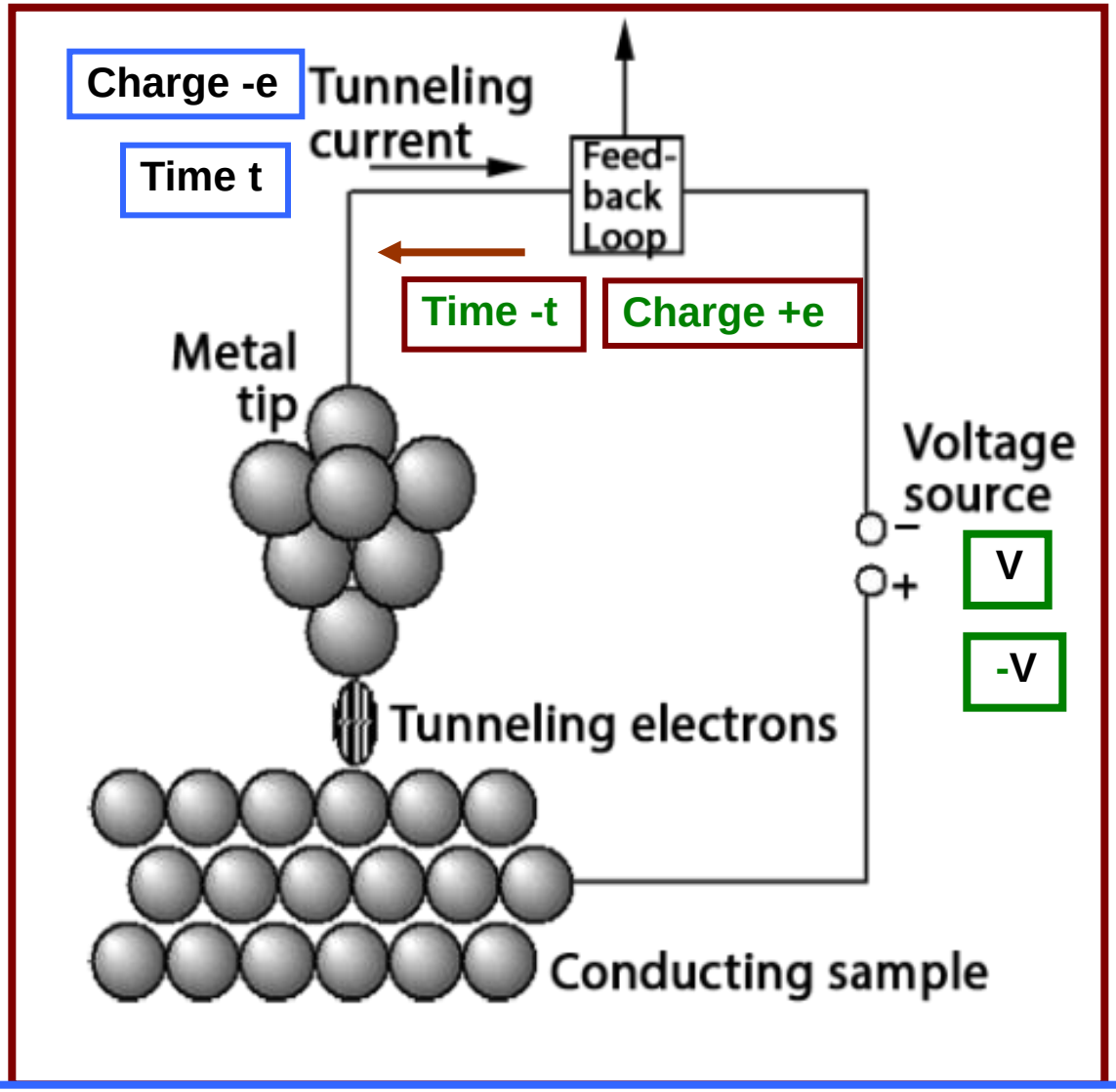

$$G(V) = \frac{dI}{dV} \propto \frac{d}{dV} \int N_{FM}(E) N_{SC}(E + eV)[f(E) - f(E + eV)]dE$$

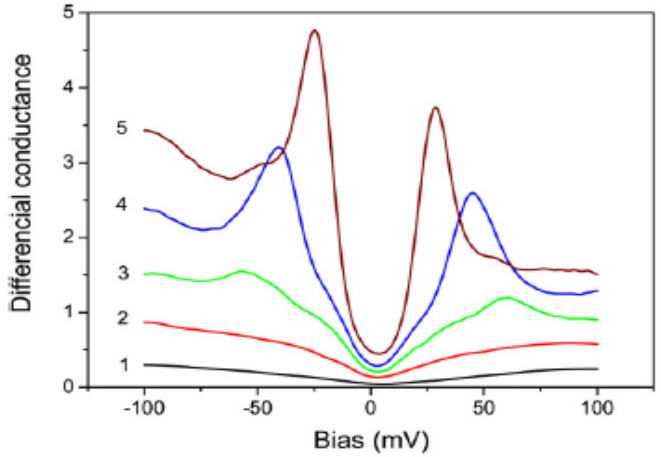

Fig. 5. Spatial variation of the tunneling differential conductance $\Delta\sigma_d(V)$ spectra measured in $Bi_2Sr_2CaCu_2O_{8+x}$. Curves 1 and 2 are taken at the positions where the integrated LDOS is very small. The low differential conductance and the absence of a superconducting gap are indicative for insulating behavior. Curve 3 is for a large gap 65 meV with small coherence peaks. The integrated value of the LDOS at the position for curve 3 is small but larger than those in curves 1 and 2. Curve 4 is for a gap of 40 meV, which is close to the mean value of the gap function. Curve 5, taken at the position with the highest integrated LDOS, is for the smallest gap of 25 meV with two very sharp coherence peaks [24].

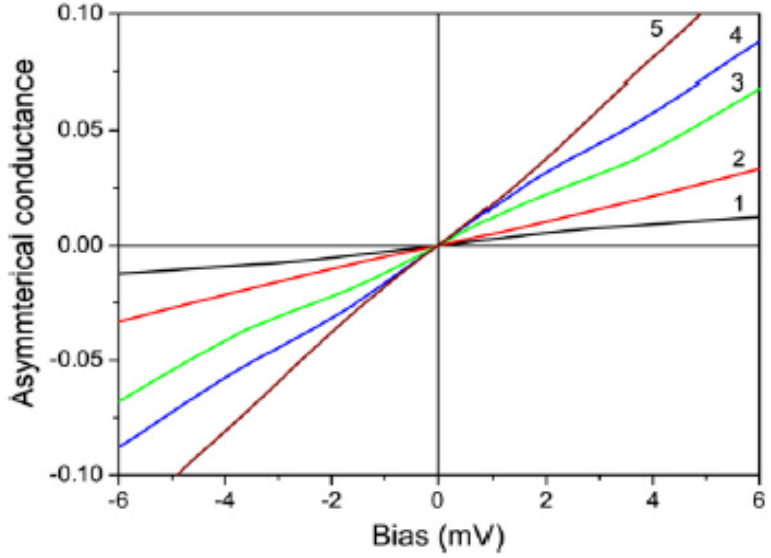

Fig. 6. The asymmetric parts $\Delta\sigma_d(V)$ of the tunneling differential conductance spectra measured in $Bi_2Sr_2CaCu_2O_{8+x}$ and extracted from data of Fig. 5 are shown as functions of the bias (mV). The number of the curve representing the asymmetric part correspond to the number of the curve displayed in Fig. 4 from which this asymmetric part was extracted.

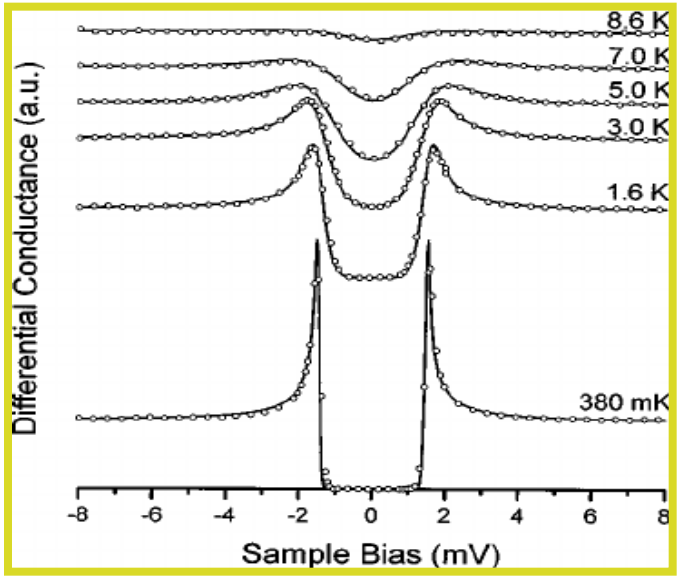

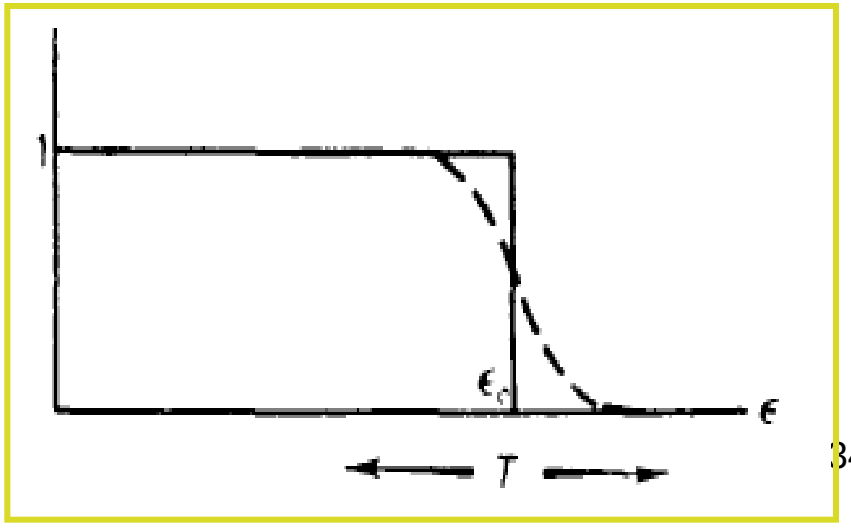

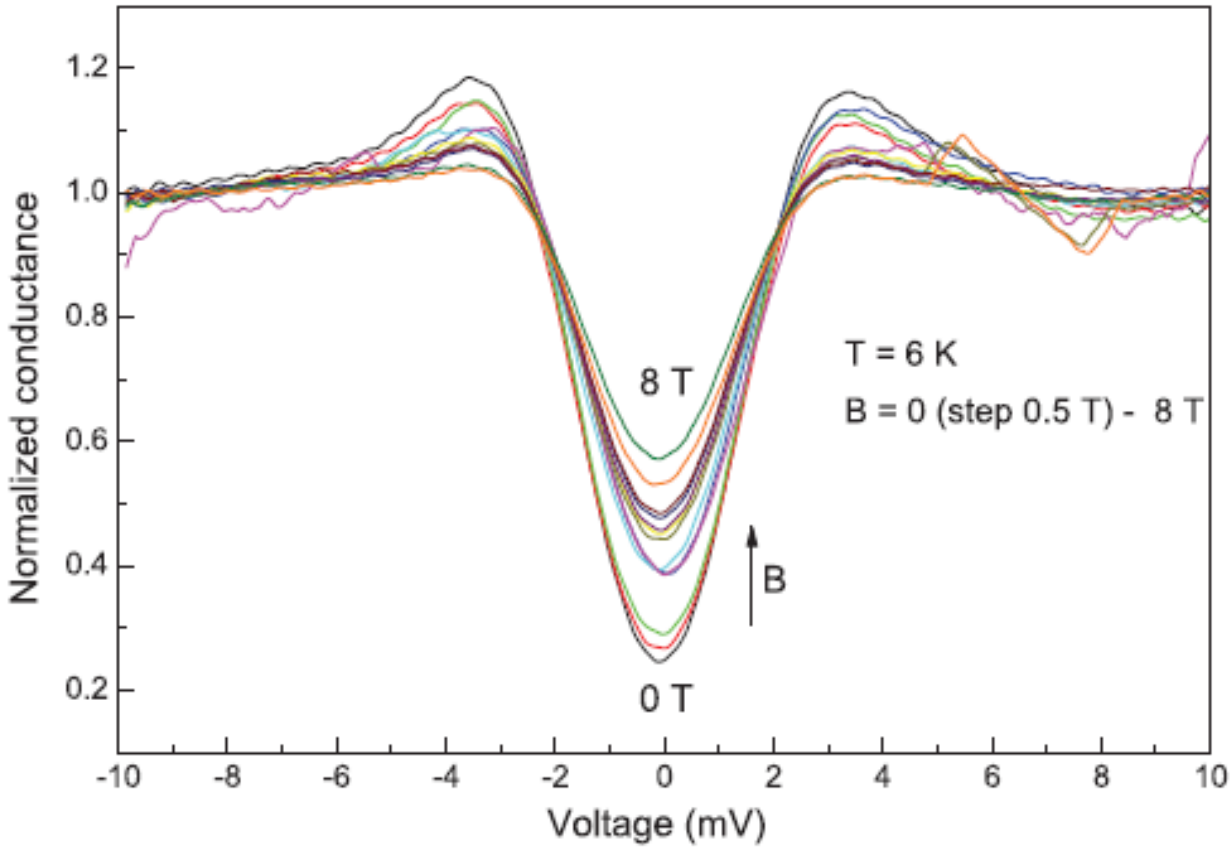

Figure 3. Differential tunneling conductance of the NbN–Au tunnel junction measured at 6 K in magnetic fields up to 8 T with a 0.5 T step.

$$\sigma_{asym} = dI(V)/dV - dI(-V)/dV.$$

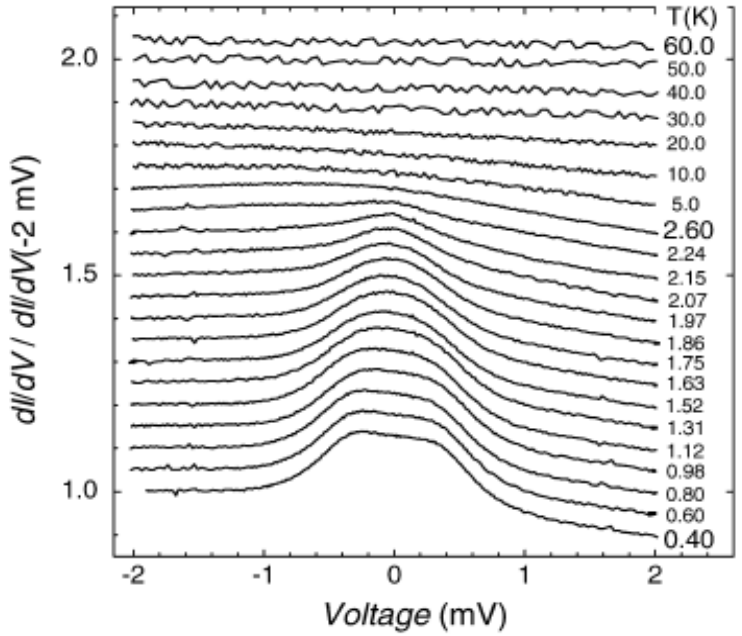

Fig. 2. Dynamic conductance spectra $\sigma_c(v) = dI/dV$ measured with point contact (Au/$CeCoIn_5$) over wide temperature range [22]. Curves $\sigma_c(v)$ are shifted vertically by 0.05 for clarity and normalized by the conductance at -2 mV. The asymmetry is seen to develop starting at 45 K and becomes stronger with decreasing temperature [22].

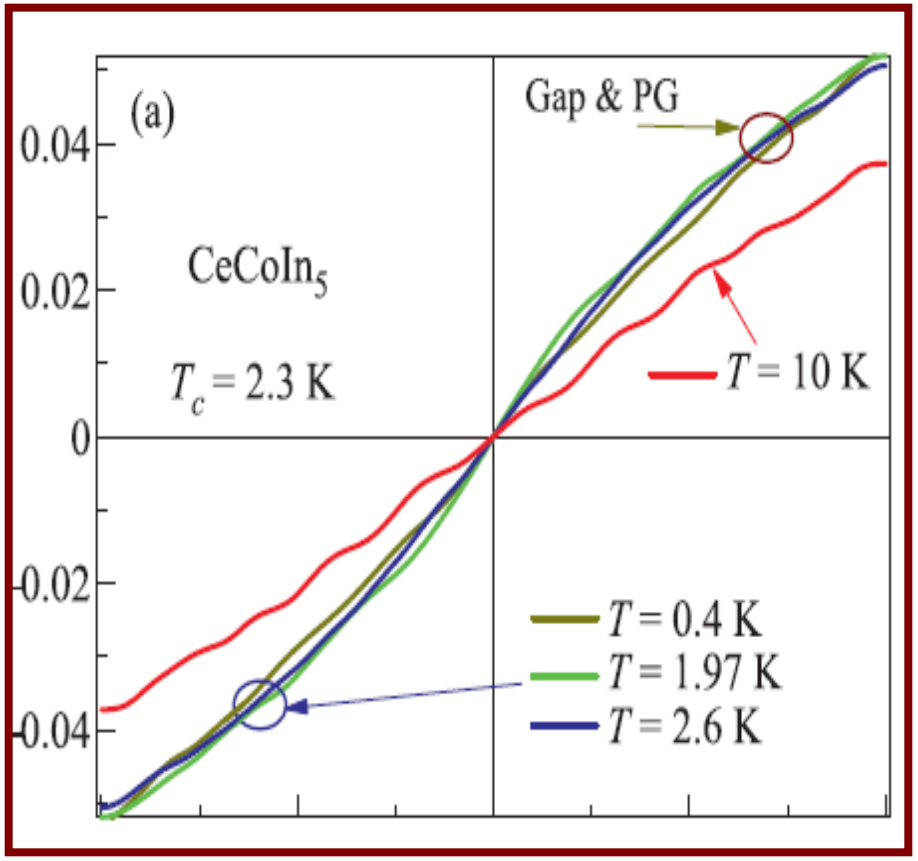

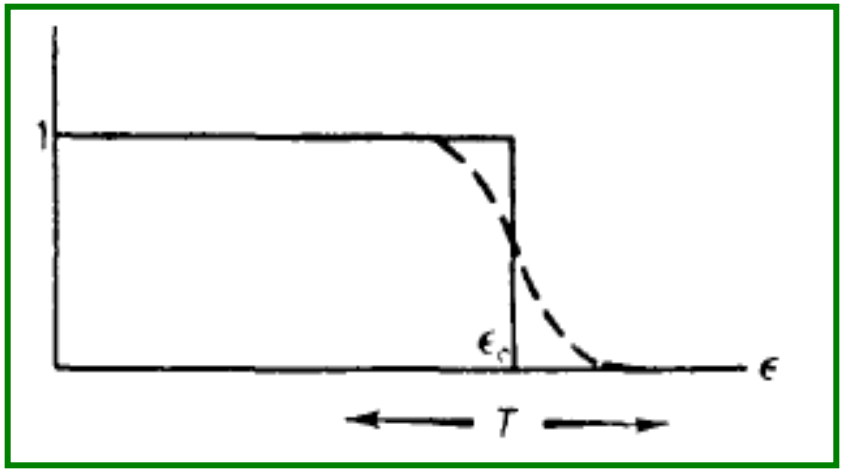

Nat. Phys. **18**, 691–698 (2022).

Interaction-driven giant thermopower in magic-angle twisted bilayer graphene
"*Emergent low-energy particle–hole asymmetry and giant thermopower peaks*"

Stepanov, P. Thermopower probes electronic flat bands. *Nat. Phys.* 18, 617–618 (2022).

Experimental facts show that the particle-hole asymmetry exists in HF compounds and is accompanied by Fermi surface transformation.
Such behavior is illuminated by the strong enhancement of the observed low-temperature value of the Seebeck coefficient.

V.A. Khodel, V.R. Shaginyan, and V.V. Khodel, New approach in the microscopic Fermi system theory, Phys. Rep. 249, 1 (1994).

to another kinetic coefficient—its thermoelectric power S_{te}, which is given by the well known integral [112]:

$$S_{te} = -\frac{2e}{3T^2\sigma}\int \omega\left(\frac{\partial\varepsilon(p)}{\partial p}\cdot \boldsymbol{L}\right)\frac{1}{[e^{\omega}/T+1][e^{-\omega/T}+1]}\frac{d^3p}{(2\pi)^3}, \qquad (7.72)$$

where $\omega = \varepsilon - \mu$ and $\boldsymbol{L}$ stands for the solution of the kinetic equation

$$I(\boldsymbol{L}) = -\boldsymbol{p}/M.$$

In a system without fermion condensate the integral written vanishes if $\boldsymbol{L}$ is replaced by a constant vector. However, in a system with fermion condensate particle and hole excitations adjacent to the Fermi surface occupy different phase volumes: the first are concentrated near the point p_f while the second are near the point p_i. As a result even if the vector $\boldsymbol{L}$ is replaced by a constant one the corresponding integral does not vanish. This means that the value of the thermoelectric power S_{te} remains nonzero at the low-temperature limit [113]. So far the experimental confirmation of this conclusion is absent.

JETP Lett. 108, 335 (2018)
Asymmetric Tunneling Conductance and the Non-Fermi Liquid Behavior of Strongly Correlated Fermi Systems

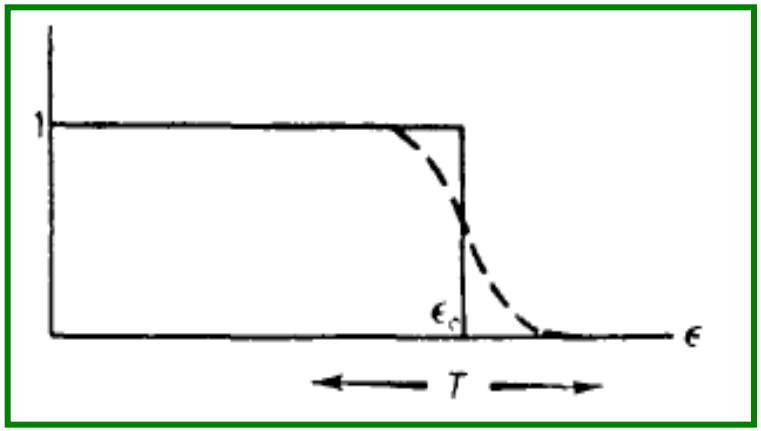

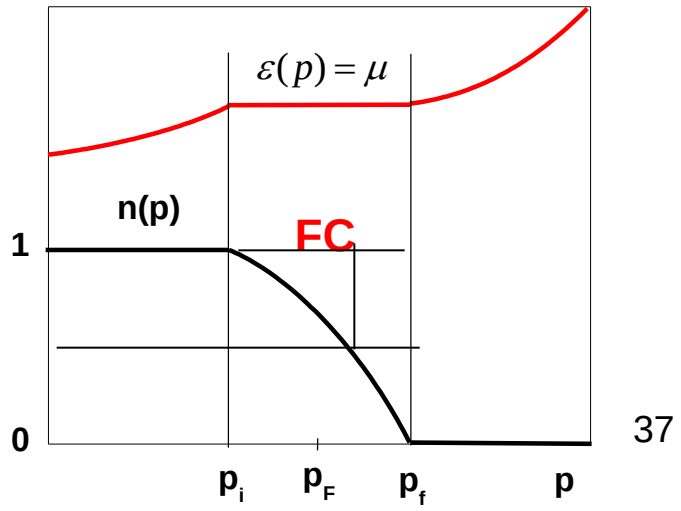

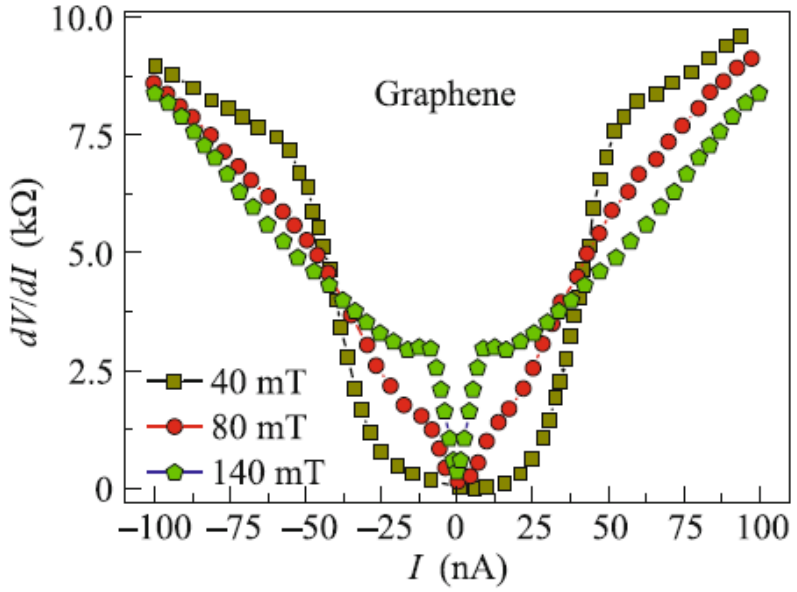

Fig. 6. (Color online) Differential resistance dV/dI as a function of bias current I versus magnetic field B shown in the legend [13]. It is seen that the asymmetry emerges at $B \leq 80\,\mathrm{mT}$ and vanishes at elevated magnetic fields

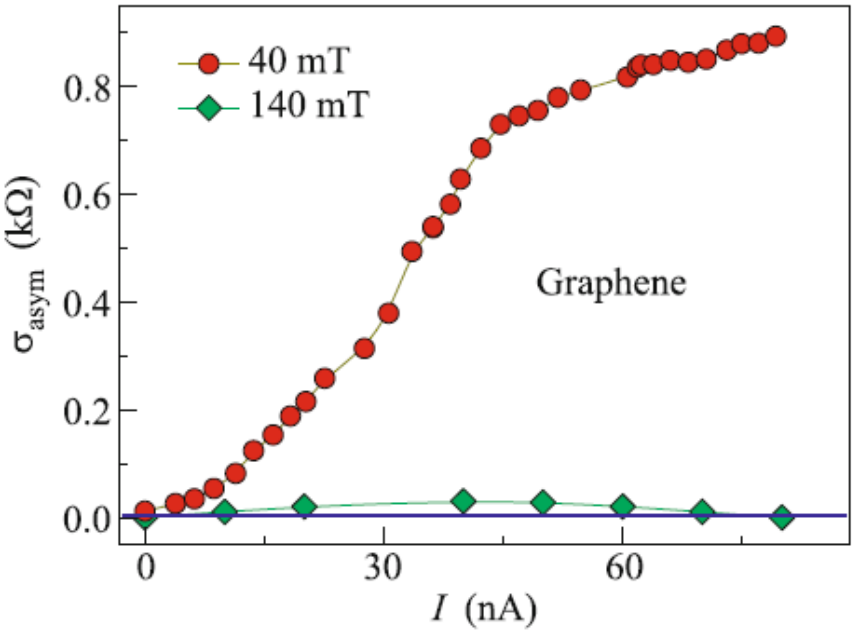

Fig. 7. (Color online) The asymmetric part of the differential resistance $\sigma_{\mathrm{asym}}(k\Omega) = dV/dI(I) - dV/dI(-I)$ is extracted from experimental data [13] exposed in Fig. 6

Y. Cao, V. Fatemi, S. Fang, K. Watanabe, T. Taniguchi, E. Kaxiras, and P. Jarillo-Herrero,
Unconventional superconductivity in magic-angle graphene superlattices
Nature **556**, 43 (2018).

V.R. Shaginyan, ***Dissymetrical tunneling in heavy-fermion metals***, JETP Lett. **81**, 222 (2005);

V.R. Shaginyan and K.G.Popov, ***Asymmetric tunneling, Andreev reflection and dynamic conductance spectra in strongly correlated metals***, Phys. Lett. A**361**, 406 (2007);

V.R. Shaginyan, A. Z.Msezane, G. S. Japaridze, V.A. Stephanovich, and Y. S. Leevik,
Asymmetric tunneling conductance and the non-Fermi liquid behavior of strongly correlated Fermi systems, Pis'ma v ZhETF, **108**, 359 (2018).

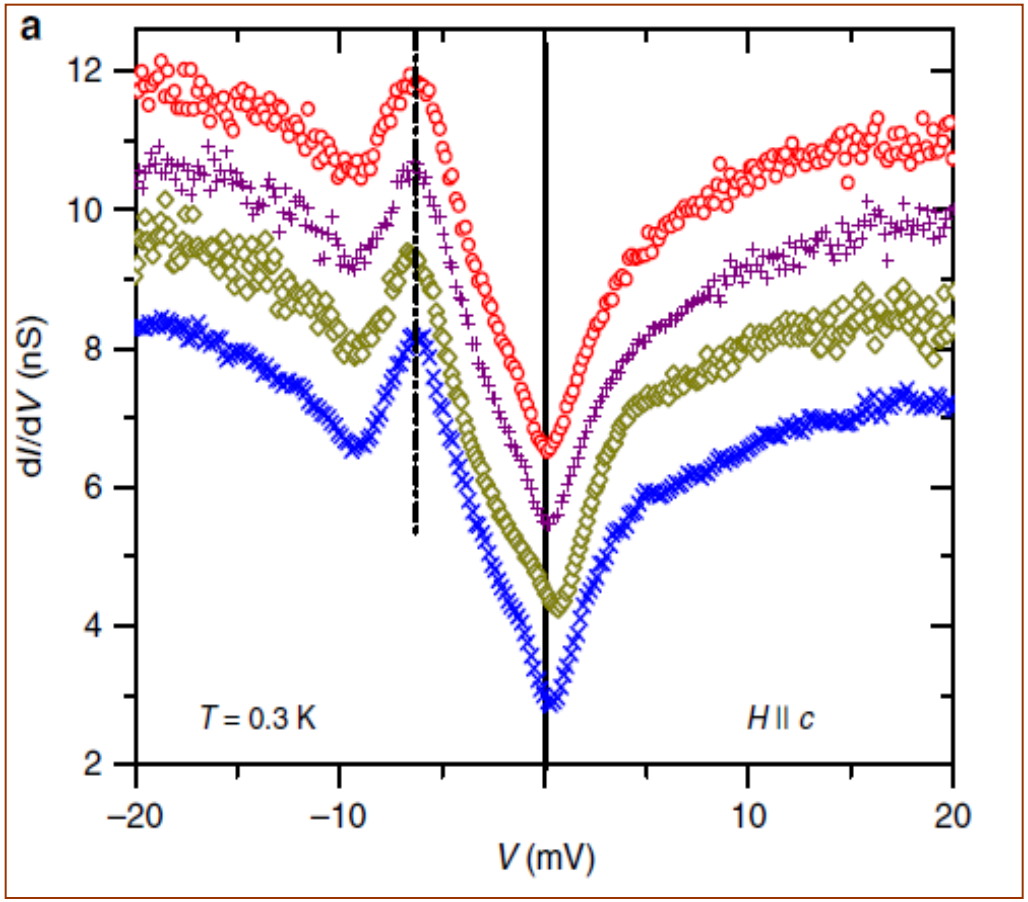

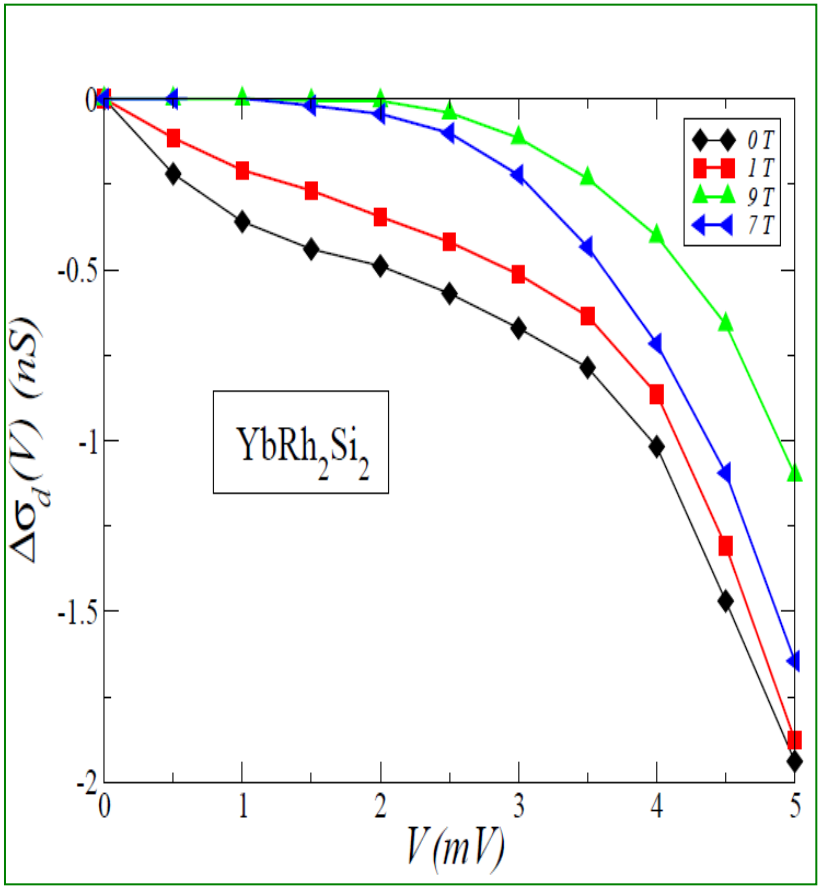

Fig. 5 Spectroscopy in applied field. **a** Tunneling conductance $g(H, T = 0.3$ K) measured at different magnetic fields (0, 1, 7, 11 T from bottom to top) applied parallel to the magnetically hard *c*-axis. Curves are offset for clarity.

Asymmetric Tunneling Conductance
and the Non-Fermi Liquid Behavior of Strongly Correlated Fermi Systems
JETP Lett. 108, 335 (2018)

V. R. Shaginyan, M. Ya. Amusia, A. Z. Msezane, and K. G. Popov, Phys. Rep. **492**, 31 (2010).

Examples of FC theory application

Scaling behavior of HF metals

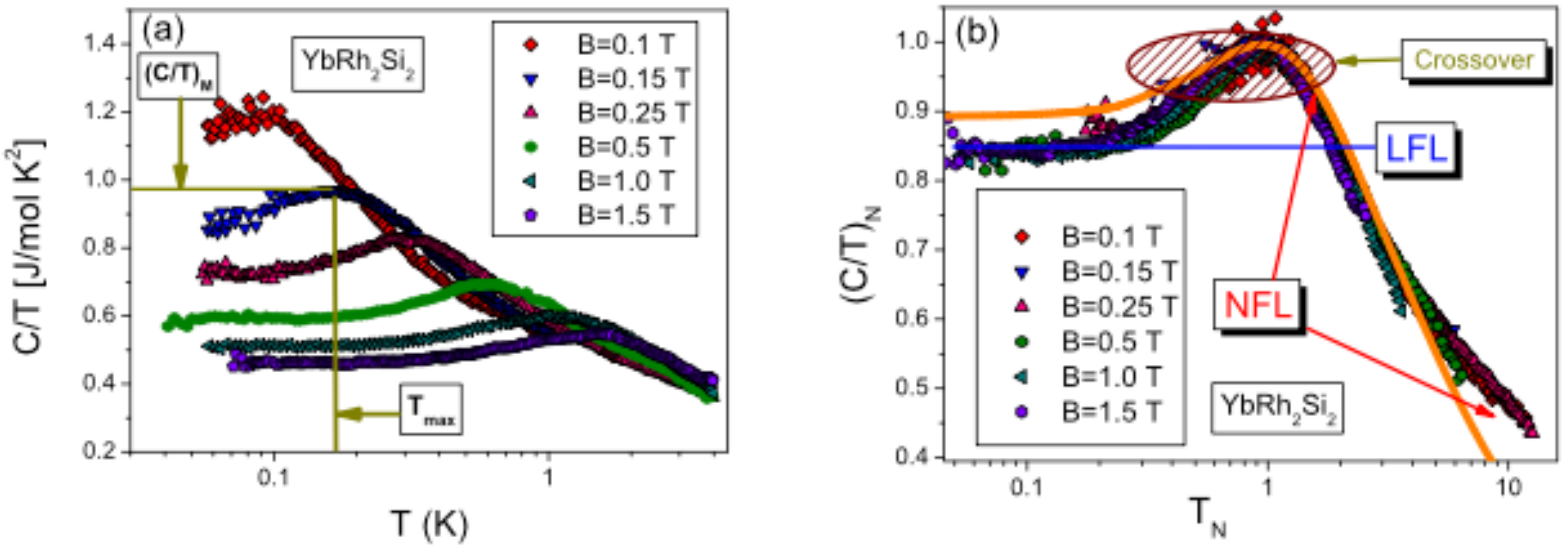

Figure 3: Scaling behavior of HF metals. Panel (a): Electronic specific heat of $YbRh_2Si_2$, C/T, versus temperature T as a function of magnetic field B [25] shown in the legend. The illustrative values of $(C/T)_M \propto M_M^*$ and T_M at $B = 0.15$ T are shown. Panel (b): The normalized effective mass M_N^* versus normalized temperature T_N. M_N^* is extracted from the measurements of the specific heat C/T on $YbRh_2Si_2$ [25], displayed in the panel (a). The constant effective mass inherent in a normal Landau Fermi liquid is presented by the solid line. The schematic crossover region is indicated by the arrow and the NFL behavior is indicated by two arrows. Our calculation based on Eq. (1) is displayed by the solid curve.

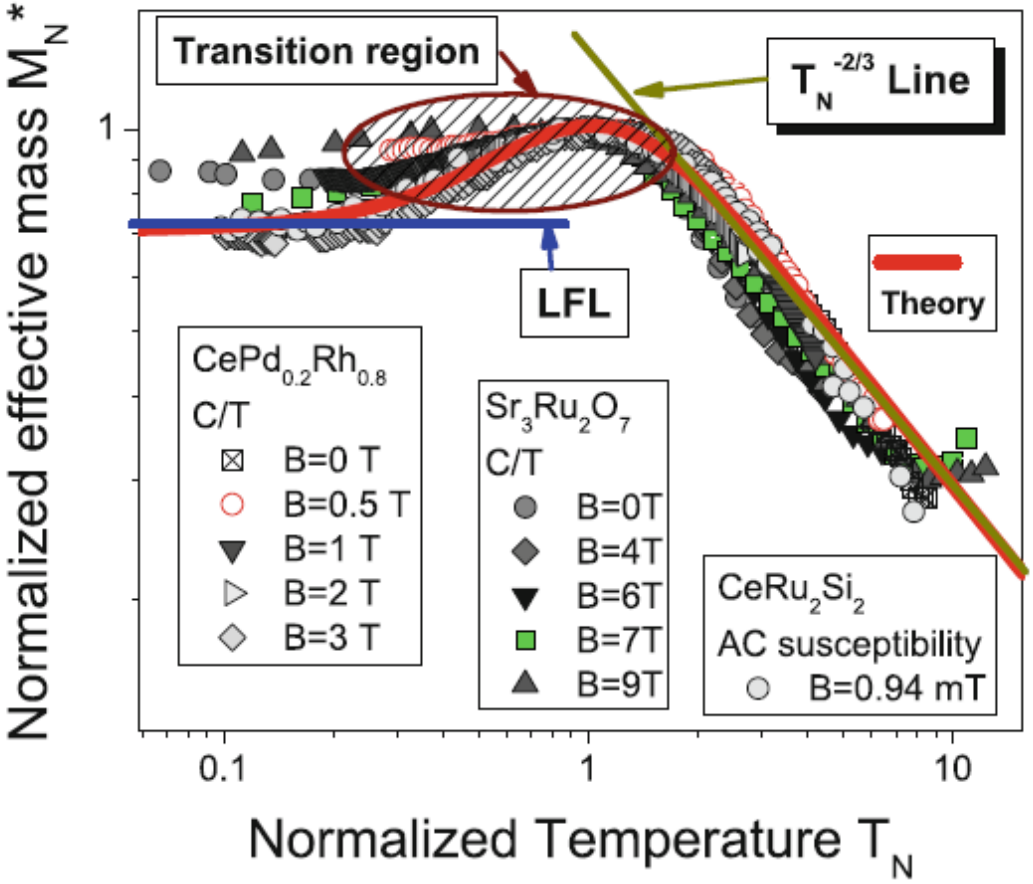

Fig. 18.6 The universal scaling behavior of the normalized effective mass M_N^* versus T_N. M_N^* is extracted from the measurements of χ and C/T (in magnetic fields B shown in the legends) on $CeRu_2Si_2$ [32], $CePd_{1-x}Rh_x$ with $x = 0.80$ [31], and $Sr_3Ru_2O_7$ [33]. The LFL and NFL regimes (latter having $M_N^* \propto T_N^{-2/3}$) are shown by the *arrows* and *straight lines*. The transition regime is depicted by the *shaded area*. The *solid curve* represents our calculation of the universal behavior of $M_N^*(T_N)$

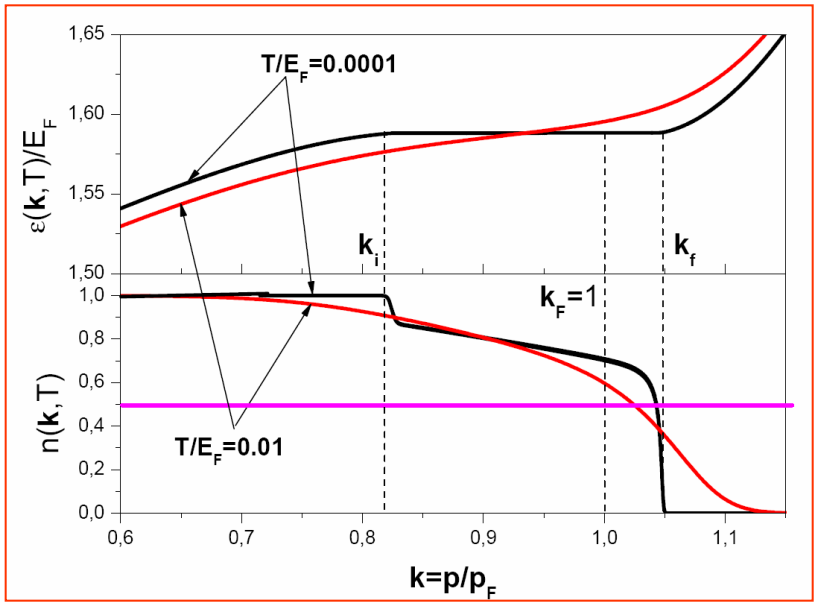

The single particle spectrum and the distribution function

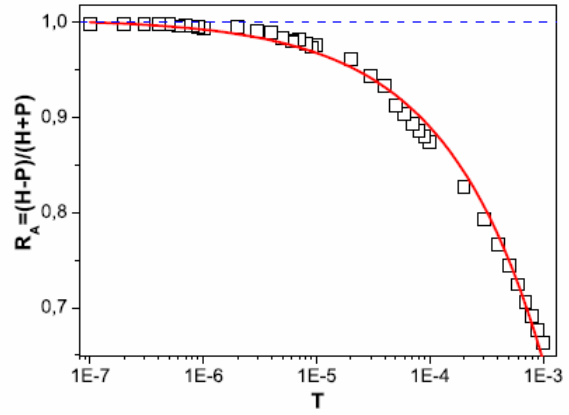

Fig. 3: (Colour on-line) R_A as a function of the dimensionless temperature measured in E_F. Our calculations are shown by squares. The solid curve represents the fit $R_A \simeq a_0 + a_1\sqrt{T}$.

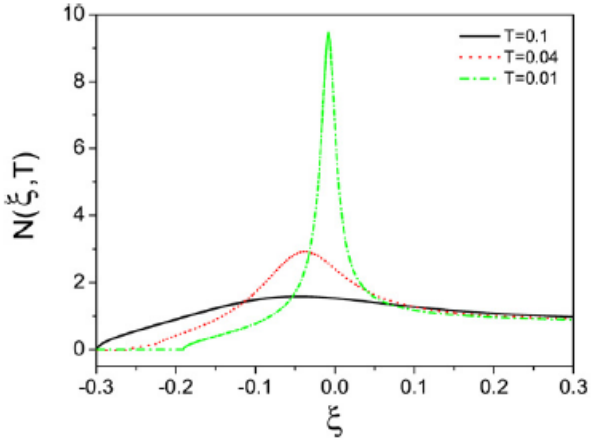

Fig. 4. The density of states $N(\xi, T)$ as a function of $\xi = (\varepsilon - \mu)/\mu$ calculated for the three values of the normalized temperature T. The values of the normalized temperature are shown in the upper right corner.

Asymmetry of the density of states

V. R. Shaginyan, G. S. Japaridze, M. Ya. Amusia, A. Z. Msezane, and K. G. Popov, Europhysics Letters **94,** 69001 (2011).

How we can solve the problem ?

Idea

- Fermion condensation quantum phase transition violates the P-H symmetry and *T* invariance
- Dark matter support the P-H violation
- Dark energy support the stability of Universe
- The P-H symmetry is violated at low temperatures *T*
- At elevated *T* the P-H symmetry is restored

At first seconds, T is higher or about the Fermi energy. The asymmetry is absent.

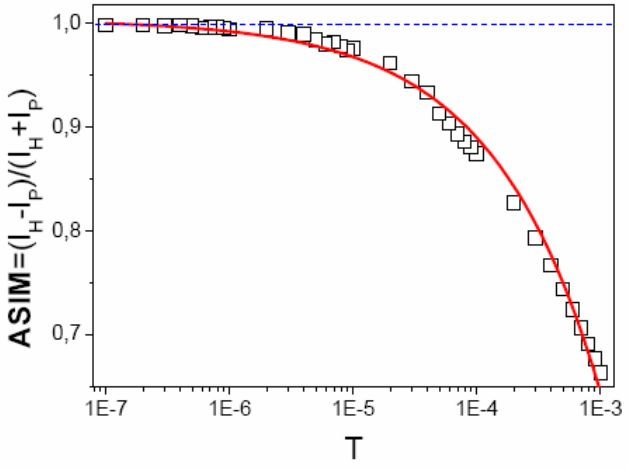

Asymmetry as a function of $T=T_0/E_F$

The dark matter forms quasiparticles. Thus the light matter matter is small part of the dark one.

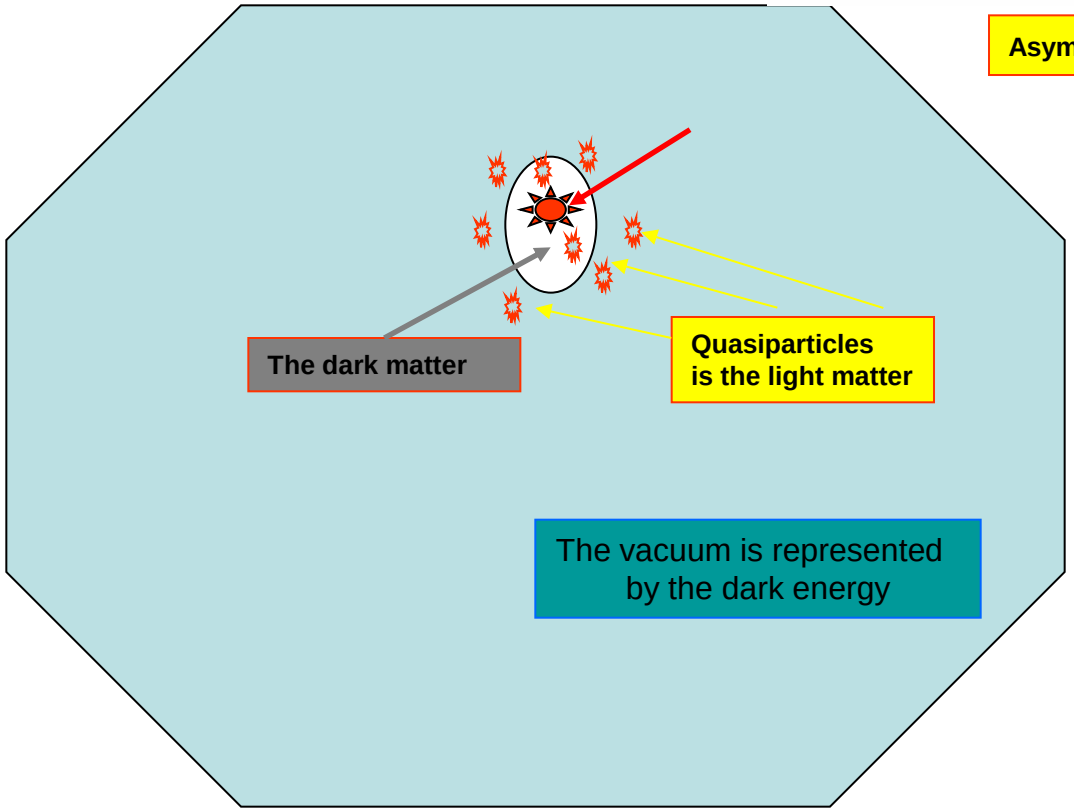

Baryon asymmetry resulting from a quantum phase transition in the early universe .

A novel mechanism for explaining the matter-antimatter asymmetry of the universe is considered. We assume that the universe starts from completely symmetric state and then, as it cools down, it undergoes a quantum-phase transition which in turn causes an asymmetry between matter and antimatter. The mechanism does not require the baryon-number–violating interactions or *CP* violation at a microscopic level. Our analysis of the matter-antimatter asymmetry is in the context of conspicuous experimental results obtained in the condensed-matter physics.

V. R. Shaginyan, G. S. Japaridze, M. Ya. Amusia, A. Z. Msezane, and K. G. Popov,
Baryon asymmetry resulting from a quantum phase transition in the early universe. EPL **94,** 69001 (2011).

V. R. Shaginyan, A. Z. Msezane, V. A. Stephanovich, G. S Japaridze, and E. Kirichenko, Flat bands and strongly correlated Fermi systems. Physica Scripta 94, 065801 (2019).

V.R. Shaginyan, A.Z. Msezane, G.S. Japaridze, and V.A. Stephanovich, Violation of the Time-Reversal and Particle-Hole Symmetries in Strongly Correlated Fermi Systems: A Review. Symmetry 12, 1596 (2020).

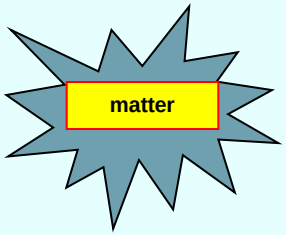

If large-scale voids are the location of antimatter.

These voids may emerge as a result of FCQPT.

The gravitational behavior of antimatter is still unknown. While we may be confident that antimatter is self-attractive, the interaction between matter and antimatter might be repulsive.

M. Villata, EPL, 94 20001 (2011).

The gravitational repulsion would prevent the mutual annihilation of isolated and alternated systems of matter and antimatter.

It was shown that voids can originate from small negative fluctuations in the primordial density field, which (acting as if they have an effective negative gravitational mass) repel surrounding matter, and grow as the largest structures in the Universe. These new cosmological scenarios could eliminate the uncomfortable presence of an unidentified dark energy, and maybe also of cosmological dark matter, which would together represent more than the 95% of the Universe content.

Piran T., Gen. Relativ. Gravit., **29,** 363 (1997).

Baryon asymmetry

Arrow of time

$$S(T \to 0) \to S_0.$$

Summary

1. **The physics of strongly correlated Fermi systems is determined by quasiparticles.**

2. **Contrary to the Landau quasiparticles, the effective mass of these quasiparticles is strongly depends on temperature, magnetic fields, density, etc.**

3. **This system of quasiparticles forms the non-Fermi liquid behavior including the particle – hole asymmetry producing CT violation at the macroscopic scale.**

4. **Baryon asymmetry, arrow of time and high entropy result from a quantum phase transition in the early universe .**


Thank you for your attention!